SYRTHES 4.2
Validation Manual

I. Rupp, C. Peniguel

2014

AVERTISSEMENT / CAUTION

Contents

AVERTISSEMENT / CAUTION 1

1 Introduction **6**

I CONDUCTION **8**

2 Introduction **9**

3 RECTAN **11**
3.1 Test case description 11
3.1.1 Geometry 11
3.1.2 Physical conditions 11
3.1.3 Initial conditions, boundary conditions 12
3.2 Analitycal solution 12
3.3 Calculation description 12
3.3.1 Meshes 12
3.4 Presentation of results 13
3.4.1 Temperature field 13
3.4.2 Comparison calculation results / analytical values 13
3.5 Synthesis 16

4 CARRE-H **17**
4.1 Test case description 17
4.1.1 Geometry 17
4.1.2 Physical conditions 17
4.1.3 Initial conditions, boundary conditions 18
4.2 Analitycal solution 18
4.3 Calculations description 18
4.3.1 Mesh 18
4.4 Presentation of results 19
4.4.1 Thermal fields at convergence 20
4.4.2 Comparison calculation results / analytical value 20
4.5 Synthesis 21

5 ANNEAU **22**
5.1 Test case description 22
5.1.1 Geometry 22
5.1.2 Physical conditions 22
5.1.3 Initial conditions, boundary conditions 23

5.2 Analitycal solution . . . 23
5.3 Calculations description . . . 23
5.3.1 Mesh . . . 23
5.4 Presentation of results . . . 24
5.4.1 Thermal fields inside the ring . . . 25
5.4.2 Comparison calculation results / analytical value . . . 25
5.5 Synthesis . . . 27

6 ANNEAU-H **28**
6.1 Test case description . . . 28
6.1.1 Geometry . . . 28
6.1.2 Physical conditions . . . 28
6.1.3 Initial conditions, boundary conditions . . . 29
6.2 Analitycal solution . . . 29
6.3 Calculations description . . . 29
6.3.1 Mesh . . . 29
6.4 Presentation of results . . . 30
6.4.1 Thermal fields inside the ring . . . 30
6.4.2 Comparison calculation results / analytical value . . . 30
6.5 Synthesis . . . 33

7 SPHERE **34**
7.1 Test case description . . . 34
7.1.1 Geometry . . . 34
7.1.2 Physical conditions . . . 34
7.1.3 Initial conditions, boundary conditions . . . 35
7.2 Analitycal solution . . . 35
7.3 Calculation description . . . 35
7.3.1 Mesh . . . 35
7.4 Presentation of results . . . 36
7.4.1 Temperature field inside the sphere . . . 36
7.4.2 Comparison calculation results / analytical values . . . 37
7.5 Synthesis . . . 38

8 BRIQUE **39**
8.1 Test case description . . . 39
8.1.1 Geometry . . . 39
8.1.2 Physical conditions . . . 39
8.1.3 Initial conditions, boundary conditions . . . 39
8.2 Analitycal solution . . . 40
8.3 Calculations description . . . 40
8.3.1 Mesh . . . 40
8.4 Presentation of results . . . 41
8.4.1 Thermal field inside the brick . . . 41
8.4.2 Comparison calculation results / analytical value . . . 41
8.5 Synthesis . . . 43

II RAYONNEMENT **44**

9 Introduction **45**

10 Calcul des facteurs de forme **47**
10.1 Facteurs de forme en dimension 3 47
10.1.1 Cas de 2 facettes en vis-à-vis 48
10.1.2 Cas de 2 facettes faisant un angle 49
10.1.3 Facteurs de forme dans un cylindre 51
10.2 Facteurs de forme en axisymétrique 52
10.2.1 Cas de 2 anneaux sur un cylindre 52
10.2.2 Cas de 2 anneaux sur un tronc de cône 53
10.2.3 Cas d'un anneau sur un cône, l'autre sur un cylindre 54
10.2.4 Cas de 2 anneaux en vis-à-vis 55
10.2.5 Traitement des faces cachées : disque perpendiculaire à un cylindre 56
10.2.6 Traitement des faces cachées : deux cylindres concentriques 58
10.2.7 Traitement des faces cachées : cône et disque 60
10.3 Synthèse de la validation des facteurs de forme 61

11 Validation du solveur **62**

12 COND_RAY **65**
12.1 Test case description 65
12.1.1 Geometry 65
12.1.2 Physical conditions 65
12.1.3 Initial conditions, boundary conditions 65
12.2 Analitycal solution 66
12.3 Calculation description 66
12.3.1 Meshes 66
12.4 Presentation of results 66
12.4.1 Comparison calculation results / analytical value 67
12.4.2 Thermal field inside plates 67
12.4.3 Study of calculation's convergence 69
12.5 Synthesis 69

13 CYLINDRES_2D_RAY **70**
13.1 Test case description 70
13.1.1 Geometry 70
13.1.2 Physical conditions 70
13.1.3 Initial conditions, boundary conditions 71
13.2 Analitycal solution 71
13.3 Calculation description 72
13.3.1 Meshes 72
13.4 Presentation of results 73
13.4.1 Temperature field inside cylinders 73
13.4.2 Comparison calculation results / analytical values 75
13.4.3 Study of calculation's convergence 75
13.5 Synthesis 76

14 SPHERE_RAY **77**
14.1 Test case description . . . 77
14.1.1 Geometry . . . 77
14.1.2 Physical conditions . . . 77
14.1.3 Initial conditions, boundary conditions . . . 78
14.2 Analitycal solution . . . 78
14.3 Calculation description . . . 79
14.3.1 Meshes . . . 79
14.4 Presentation of results . . . 80
14.4.1 Temperature field inside the spheres . . . 80
14.4.2 Comparison calculation results / analytical values . . . 81
14.4.3 Study of calculation's convergence . . . 82
14.5 Synthesis . . . 83

15 CYLINDRES_3D_RAY **84**
15.1 Test case description . . . 84
15.1.1 Geometry . . . 84
15.1.2 Physical conditions . . . 84
15.1.3 Initial conditions, boundary conditions . . . 85
15.2 Analitycal solution . . . 85
15.3 Calculation description . . . 86
15.3.1 Meshes . . . 86
15.4 Presentation of results . . . 87
15.4.1 Temperature domains inside cylinders . . . 87
15.4.2 Comparison calculation results / analytical values . . . 87
15.4.3 Study of calculation's convergence . . . 88
15.5 Synthesis . . . 88

III TRANSFERTS COUPLES **90**

16 WOODPANEL **91**
16.1 Test case description . . . 91
16.1.1 Geometry . . . 91
16.1.2 Physical conditions . . . 91
16.1.3 Boundary conditions . . . 92
16.2 Calculation description . . . 92
16.2.1 Meshes . . . 92
16.3 Presentation of results . . . 92

Chapter 1

Introduction

SYRTHES (SYstème de Résolution THErmique Solide) est un code généraliste de thermique qui permet d'étudier des configurations industrielles très variées.

Il a pour objectif de résoudre les problèmes thermiques faisant intervenir de la conduction et du rayonnement confiné de paroi à paroi.

Plusieurs documents permettent de cerner les potentialités de SYRTHES :

- un manuel utilisateur [4] (comprenant un certain nombre d'exemples),
- un manuel théorique [5] (méthodes et choix retenus pour la modélisation des phénomènes),
- des articles qui présentent notamment de nombreux cas industriels, dans le domaine du nucléaire, des applications de l'électricité et plus généralement dans des configurations où la thermique est importante ([8],[10],[9], [11],[12],[13],[2], [7],[1],[3]).

Dans la mesure où SYRTHES intervient dans de nombreuses études à caractère industriel, les auteurs ont toujours (dans la mesure des moyens disponibles) apporté un soin particulier à la qualité des résultats fournis par le code.

Cette étape est d'autant plus importante que SYRTHES peut intervenir comme un maillon dans une chaîne logicielle complexe pouvant faire intervenir un code de neutronique (TRIPOLI), un code de mécanique des fluides (actuellement *Code_Saturne* ou NEPTUNE), et un code de mécanique (*Code_Aster*).

Le travail associé à la validation de SYRTHES a été volontairement découpé en deux phases dont les finalités sont assez distinctes même si elles peuvent parfois se recouvrir mutuellement,

- une première phase consiste à s'assurer que les approches retenues et les méthodes mises en œuvres (modélisations, méthodes numériques, codage) donnent des résultats fiables et rigoureux. C'est l'objectif de ce document, qui peut à ce titre être considéré comme une "validation élémentaire" des méthodes implantées dans le code.
- une seconde phase (qui, en toute rigueur ne peut intervenir qu'à l'issue de la première étape) consiste à élaborer une base de validation où l'on cherche à vérifier le "bon fonctionnement" du code. Cette validation, à caractère plus "industriel et automatique", porte sur un ensemble de configurations plus ou moins nombreuses et complexes, (suivant l'investissement que l'on est prêt à faire dans cette partie du projet). Cette partie sera réalisée dans un second temps et fera l'objet d'un document spécifique.

Pour l'étape de validation élémentaire, le critère retenu est de tester les méthodes (parfois assez novatrices) implantées dans SYRTHES. Il faut pour cela pouvoir comparer les résultats obtenus à des solutions de référence connues sans aucune ambiguïté et avec une grande précision. Au moins dans un premier temps, cela a conduit les auteurs à ne retenir que des configurations disposant de solutions analytiques.
En conduction, la référence [14] est particulièrement mise à contribution. En rayonnement, on s'est principalement appuyé sur la référence [15].

Le rapport est divisé en deux parties distinctes, la première est dédiée à la validation de la résolution de la conduction, la seconde s'attache plus particulièrement au problème du rayonnement et du couplage des deux phénomènes.

Parmi les fonctionnalités testées, on pourra citer en particulier :

- l'obtention d'états permanents en géométries 2D cartésiennes, 2D axisymétriques et 3D,
- la prise en compte de conditions aux limites de type Dirichlet, flux, échange,
- l'influence du maillage sur les résultats,
- la prédiction d'états transitoires et permanents en configurations axisymétriques et tridimensionnelles,
- pour le rayonnement, le calcul de quantités géométriques (les facteurs de forme) dans de nombreuses situations élémentaires,
- le calcul de solutions stationnaires faisant intervenir le couplage entre rayonnement et conduction.

Part I

CONDUCTION

Chapter 2

Introduction

On cherche, dans cette première partie à tester les méthodes et algorithmes relatifs à la résolution de la conduction dans les solides. Cela comprend entre autres :

- la lecture des maillages,
- le calcul des matrices élémentaires,
- la prise en compte de conditions aux limites diverses (Dirichlet, flux,...)
- la résolution du système conductif (partie solveur),
- l'écriture des résultats.

Cette première partie est résolument indépendante des aspects radiatifs car de nombreuses configurations industrielles ne font appel qu'aux aspects conductifs.
Dans la mesure où la méthodologie retenue au sein du code découple numériquement ces deux aspects, il est légitime de les tester de façon indépendante.

On va présenter quelques cas qui permettent de tester en particulier :

- la discrétisation 2D cartésienne,
- la discrétisation 2D axisymétrique,
- la discrétisation 3D,
- les conditions de Dirichlet,
- les conditions d'échange,
- l'influence du raffinement des maillages,
- l'influence du pas de temps.

L'obtention de solutions analytiques pose des problèmes dès que le cas se complexifie. En particulier, on observe que l'on ne propose pas de solution pour les matériaux anisotropes ou dont les caractéristiques physiques (masse volumique, chaleur spécifique, conductivité) dépendent de la température via une fonction (ce qui induit une non linéarité).
La mise en œuvre dans SYRTHES de telles configurations est immédiate mais les solutions analytiques auxquelles on voudrait se comparer manquent alors.

Dans le cadre spécifique de SYRTHES, on rappelle toutefois que les méthodes utilisées et les chemins informatiques empruntés sont identiques que les propriétés soient variables ou non ce qui permet d'être confiant quant aux résultats fournis par le code.

Toute solution analytique pour des cas instationnaires et "non linéaires" est la bienvenue...
De tels cas seraient alors testés et introduits au fur et à mesure qu'ils seraient portés à la connaissance des auteurs dans cette base de validation élémentaire.

Chapter 3

RECTAN

Characteristics : 2D, steday state, boundary conditions = imposed temperature

Objectives : Validation of thermal resolution inside a solid in 2D for a staedy state. Validation of the treatment of Dirichlet's conditions.

3.1 Test case description

3.1.1 Geometry

Consider a rectangle which dimension are $0 < x < 1\ m$, $0 < y < 2\ m$.

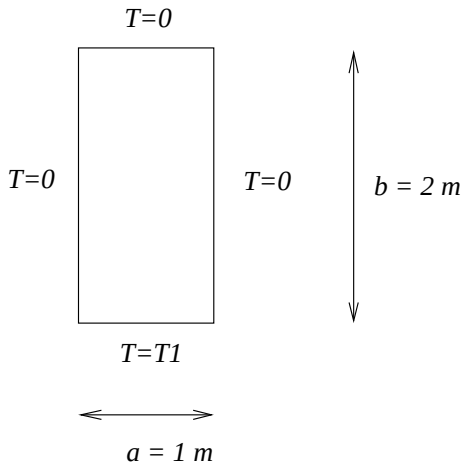

Figure 3.1: Solid domain

3.1.2 Physical conditions

The solid is related to steel having following physical characteristics :

- conductivity $k = 25\ W/mK$
- density $\rho = 7700\ kg/m^3$
- specific heat $C_p = 460\ J/kgK$

3.1.3 Initial conditions, boundary conditions

Initialy (at $t = 0$), the solid is at $20°C$.
We impose on the lower side ($y = 0$) a temperature T_1=$1°C$ and on the three other sides a temperature equal to $0°C$.

3.2 Analitycal solution

In the case of a plate of size $0 < x < a$ and $0 < y < b$ subject to following conditions : temperature T_1 en $y = 0$ and null temperature on the 3 other sides, the temperature in a point (x, y) of the plate is given by :

$$T(x,y) = \frac{4T_1}{\pi} \sum_{n=0}^{\infty} \frac{1}{2n+1} \, sin\frac{(2n+1)\pi x}{a} \, sinh\frac{(b-y)(2n+1)\pi}{a} \, cosech\frac{(2n+1)\pi b}{a}$$

3.3 Calculation description

3.3.1 Meshes

The mesh has :

- 3081 nodes with 800 vertex nodes,
- 1482 triangles.

Border nodes $y = 0$ have reference 1, those of other sides reference 2, others reference 0.

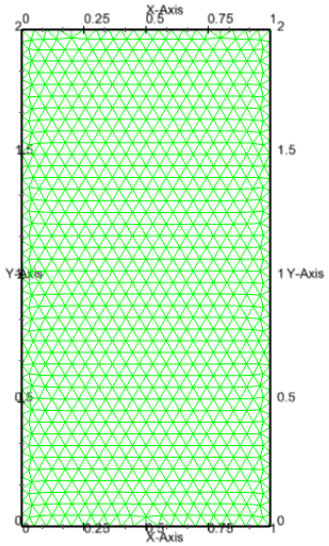

Figure 3.2: Mesh

3.4 Presentation of results

Steady state is reached after about 1.5 days.
For numerical simulation, we have used a time step equal to 500 seconds and convergence is reached after about 250 time steps.

3.4.1 Temperature field

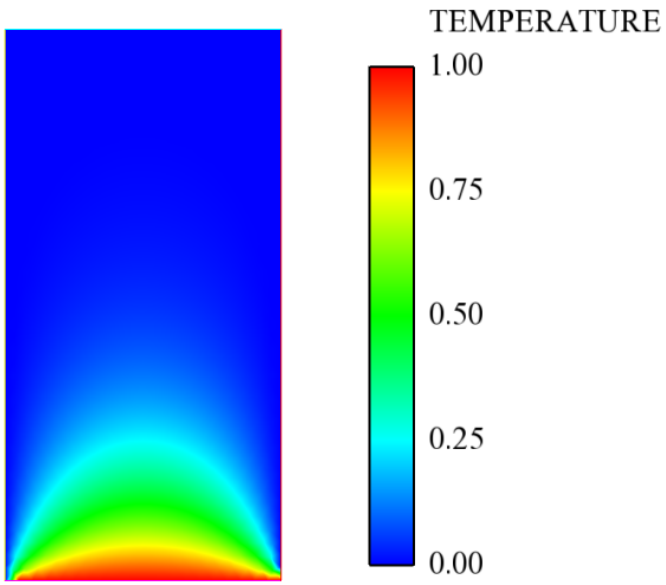

Figure 3.3: Temperature field at convergence

3.4.2 Comparison calculation results / analytical values

At convergence, comparison of calculated profiles and analytical ones.

On figures 3.8 and 3.9 one compares on 2 given points the temperature calculated (steady value reached at the end of the transient) and the analytical value (exact solution of temperature).

The two nodes that were selected are: node 366 of coordinates $(0.4736842, 0.2564102)$ node 393 of coordinates $(0.4736841, 1.6410300)$

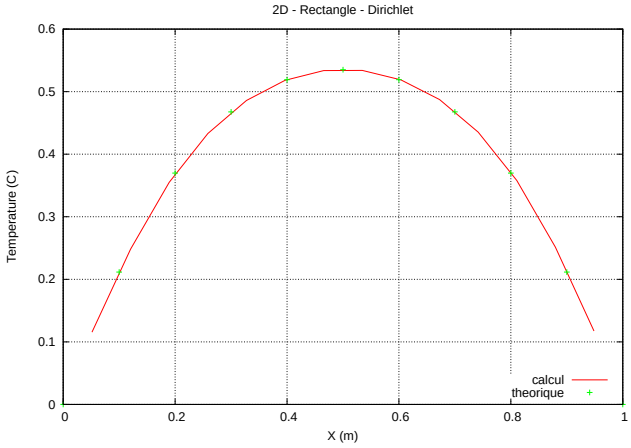

Figure 3.4: Temperature profiles at Y = 0.2564 m

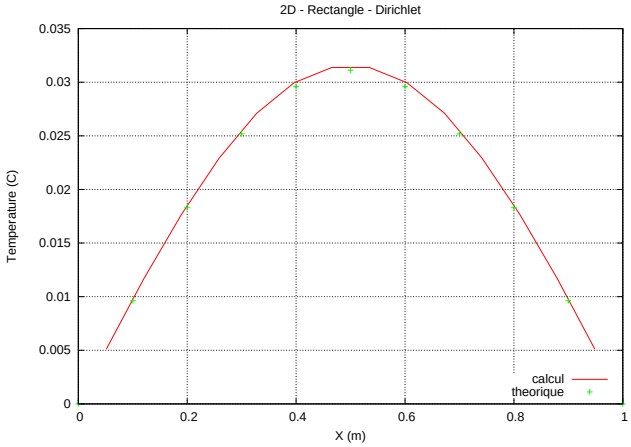

Figure 3.5: Temperature profiles at Y = 1.1795 m

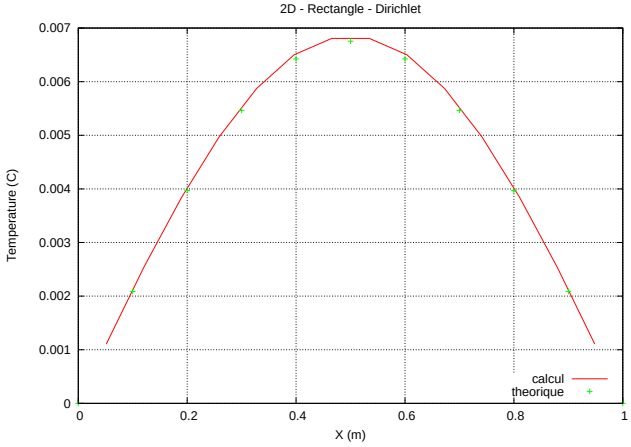

Figure 3.6: Temperature profiles at Y = 1.64103 m

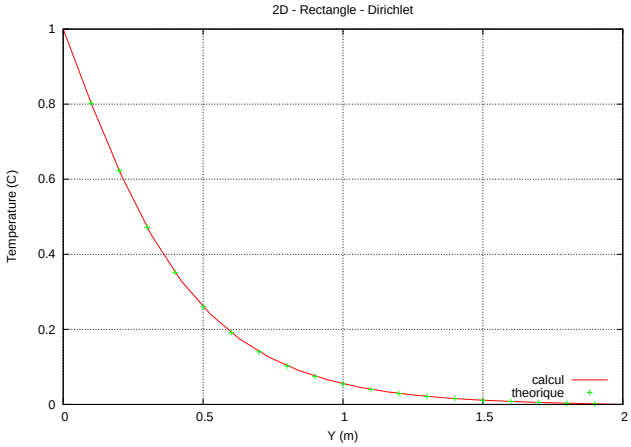

Figure 3.7: Temperature profiles at X = 0.4736842 m

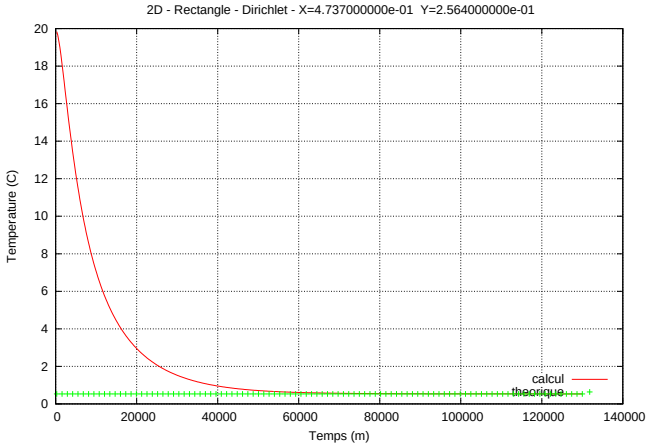

Figure 3.8: Convergence at node 366 x=0.4737 y=0.2564

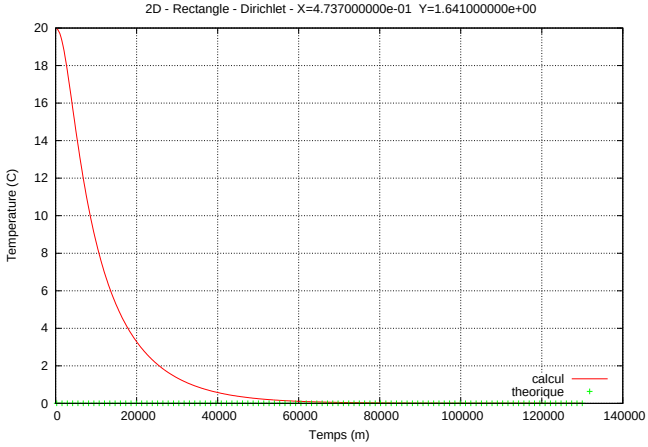

Figure 3.9: Convergence at node 393 x=0.4737 y=1.6410

Remarks :
Error values shown on the curves correspond to the absolute value of temperature deviation between theoretical value and calculated value divided by maximum temperature deviation observed on the studied configuration. It can effectively provide a better estimate of the "relative" error committed for a given configuration. Indeed, relative error built by the ratio between temperature deviation by the temperature value at considered point maximizes totally artificially committed error when the theoretical temperature tends to 0. Conversly, a calculation made between two high temperatures would lead to estimate (again, artificially) a relative error much lower.

3.5 Synthesis

The elementary case RECTAN gives satisfactory solution. It allows to test particularly calculations of elementary matrices in 2D cartesian and boundary conditions of Dirichlet type.

Strictly speaking, the mesh is not necessarily optimal for the accepted simulation. In the frame of a study, it would be preferable to densify mesh at lower level corners where the temperature field is singular and where temperature gradients are very important. Inversely, the mesh could be looser int he upper portion.

Chapter 4

CARRE-H

Characteristics : 2D, steady state, boundary conditions of mixed type, Dirichlet and exchange coefficient.

Objectifs : Validation of thermal resolution inside a solid in dimension 2 for a steady state. Validation of the treatment of boundary conditions of exchange and Dirichlet type.

4.1 Test case description

4.1.1 Geometry

Consider a square of 1m side.

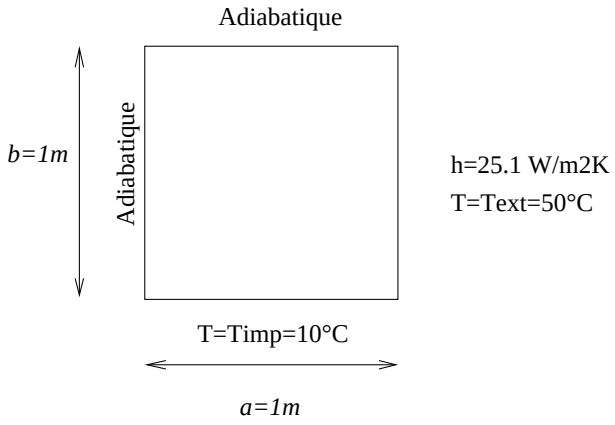

Figure 4.1: Solid domain

4.1.2 Physical conditions

The solid is related to steel having following physical characteristics :

- conductivity $k = 25.1\ W/mK$
- density $\rho = 7700\ kg/m^3$
- specific heat $C_p = 460\ J/kgK$

4.1.3 Initial conditions, boundary conditions

Initialy (at $t = 0$), the solid is at $20°C$.
We impose on the lower side ($y = 0$) a temperature T_1=$10°C$ and on the right side ($x = 1$) a condition of exchange type, with $h = 25.1\ W/m^2K$ and the environment is at a temperature of $50°C$.

4.2 Analitycal solution

In case of a plate of size $0 < x < 1$ and $0 < y < 1$ subject to following condition : temperature $T = T_{imp}$ in $y = 0$ exchange condition of type $h(T_{ext} - T)$ on side $x = 1$ and null flux condition on others sides, temperature at point (x, y) of the plate is given by :

$$T(x,y) = T_{ext} + 2h(T_{imp} - T_{ext}) \sum_{n=1}^{\infty} \frac{cos\ \alpha_n x\ \ cosh\ \alpha_n(1-y)}{[\ (\alpha_n{}^2 + h^2) + h]\ cos\ \alpha_n\ \ cosh\ \alpha_n}$$

where α_n are roots of following transcendental equation :

$$\alpha_n\ tan\ \alpha_n = 1$$

It reminds values (approximated) des 9 first roots :

$$\begin{aligned}
\alpha_1 &= 0.8603 \\
\alpha_2 &= 3.4256 \\
\alpha_3 &= 6.4373 \\
\alpha_4 &= 9.5293 \\
\alpha_5 &= 12.6453 \\
\alpha_6 &= 15.7713 \\
\alpha_7 &= 18.9025 \\
\alpha_8 &= 22.0365 \\
\alpha_9 &= 25.17245
\end{aligned}$$

4.3 Calculations description

4.3.1 Mesh

Mesh has :

- 40 401 nodes with 10 201 vertex nodes
- 20 000 triangles

Nodes of the edge $y = 0$ has reference 1, those affected by the exchange coefficient have reference 3.

We note that the used mesh is very fine. Logically, physics of the problem does not impose a so fine spatial discretization (except maybe at the bottom right corner where temperature gradients are severe). On the other hand, this mesh permit to do an informatic test with a more important number of nodes.

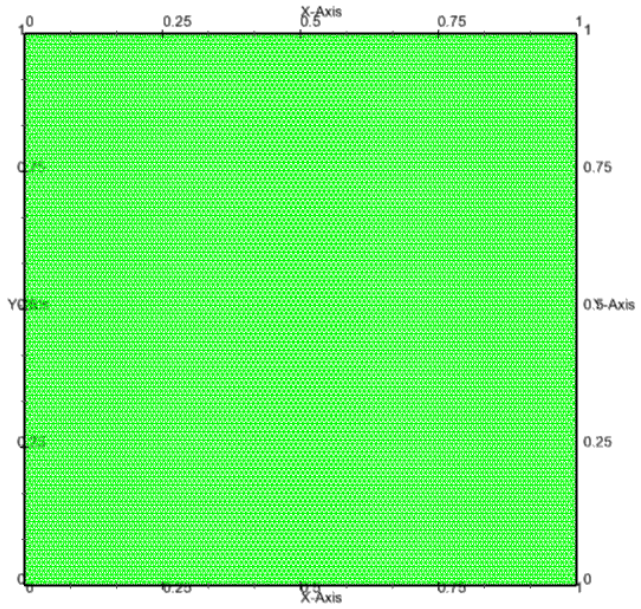

Figure 4.2: Square's mesh

4.4 Presentation of results

To reach the steady state, the chosen time step is high (1000s). If we wanted to simulate accurately an unstationnary evolution, it would be desirable to reduce a little bit this value.

It takes about 3.5 days (physical time) to reach the steady state.
The calcultaion needs about 300 time steps.

4.4.1 Thermal fields at convergence

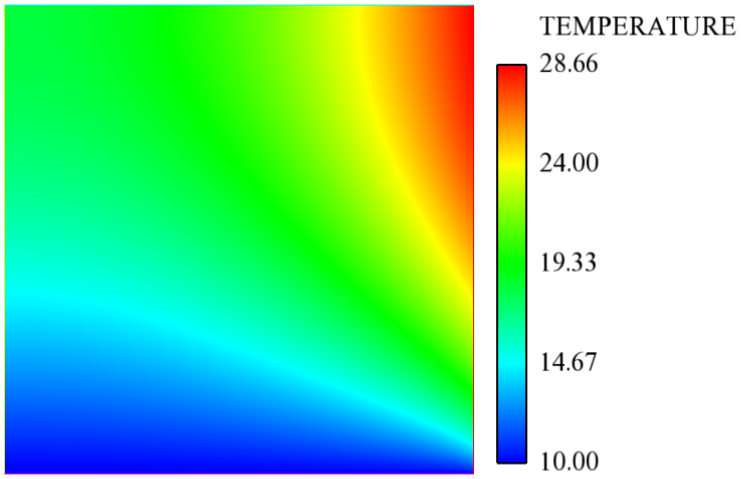

Figure 4.3: Thermal fields at convergence

4.4.2 Comparison calculation results / analytical value

We present 2 temperature profiles. Firts one is along the direction x (horizontal), it has ordinate $y = 0.5$, second one along the direction y (vertical) and has for abscisse $x = 0.5$

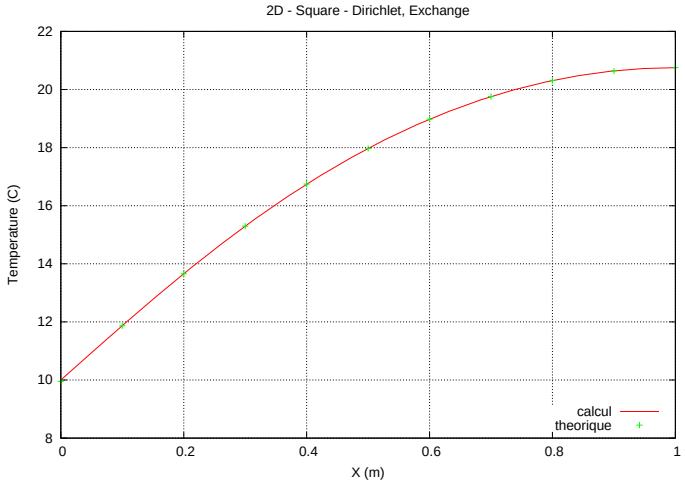

Figure 4.4: Temperature profile at Y = 0.5 m

Remarks :
Prediction is obtained with a precision of about 0.05% compared to analytical solution, but note

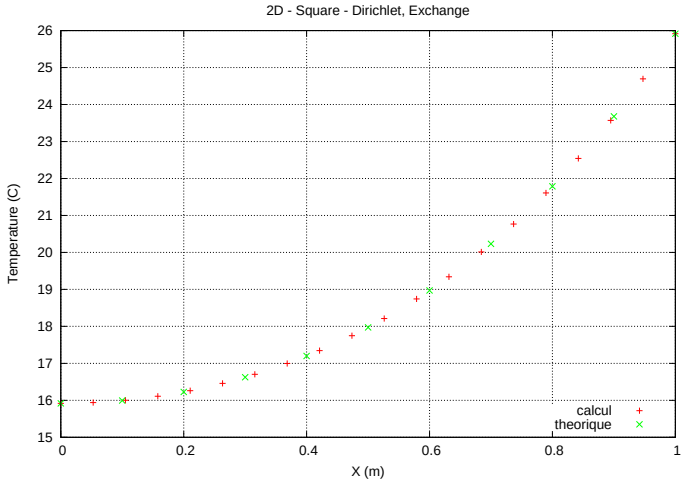

Figure 4.5: Temperature profile at X = 0.5 m

that theoretical formula is only guaranteed to a precision of this order also, The fact that the series is troncated to the ninth term and that the transcendental equation's roots have been computed to the fourth decimal.

4.5 Synthesis

The case CARREH give satisfactory results. It permits to test elementary matrices's calculation in 2D cartesian on a well fine mesh but especially, it permits to test boundary conditions of exchange type.
We check also that mixed conditions within one calculation (Dirichlet/exchange) are correctly understood.

TH retained mesh is much more fine than configuration requirement (except maybe at the bottom right corner) but this permits to test conmputantionally a case with a number of nodes more related with those used in the industriel computing.

Chapter 5

ANNEAU

Features : 2D, steady state, boundary condition = imposed temperature

Objectifs : Validation of thermal resolution inside a 2D solid for a steady state. Validation of Dirichlet conditions's processing. Influence of mesh's fineness.

5.1 Test case description

5.1.1 Geometry

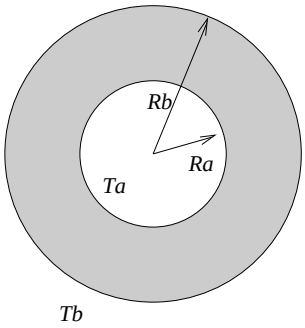

Figure 5.1: Solid domain

We consider a ring whose dimension are :

- inner radius $R_a = 0.5m$
- outer radius $R_b = 1m$

5.1.2 Physical conditions

The solid is related to steel having following physical characteristics :

- conductivity $k = 25\ W/mK$
- density $\rho = 7700\ kg/m^3$
- specific heat $C_p = 460\ J/kgK$

5.1.3 Initial conditions, boundary conditions

Initially (at $t = 0$), the solid is at $20°C$.
We impose on the inside of the ring a temperature $T_a = 10°C$ and on the outside a temperature $T_b = 50°C$.

5.2 Analitycal solution

In case of a small radius ring R_a and large radius R_b, which inside temperature is imposed at T_a and outside temperature at T_b we obtain, at steady state, the temperature to a point located at a radius r as follows :

$$T(r) = \frac{T_a \ \log(\frac{R_b}{r}) \ + \ T_b \ \log(\frac{r}{R_a})}{\log(\frac{R_b}{R_a})}$$

5.3 Calculations description

5.3.1 Mesh

Two meshes have been made in order to test influence of ladders's size on results.

The coarse mesh has :

- 2 888 nodes with 760 vertex nodes,
- 1 368 triangles.

For the fine mesh, we have divided the ladders's size by 2. It has :

- 12 168 nodes dont 3 120 vertex nodes,
- 5 928 triangles.

In both cases, internal boarder nodes has reference 1, those of external boarder reference 2, others reference 0.

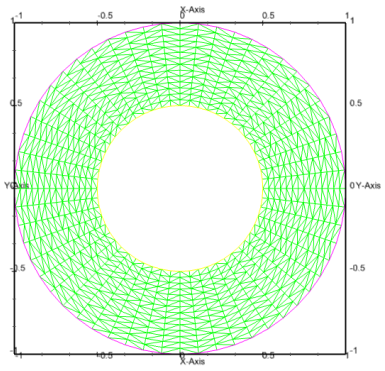

Figure 5.2: Coarse mesh

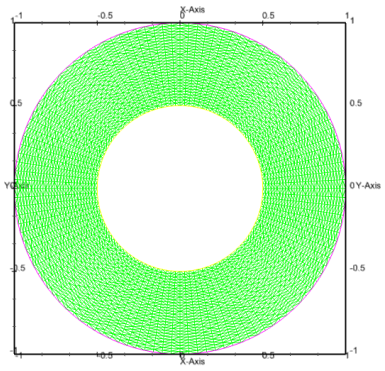

Figure 5.3: Fine mesh

5.4 Presentation of results

Steady state is obtained after about 1 hour of physical time. For both meshes, we have used a time step equal to 100 seconds. For the coarse mesh, convergence has been reached after nearly 350 time steps. For the fine mesh, steady state is obtained after nearly 350 time steps.

5.4.1 Thermal fields inside the ring

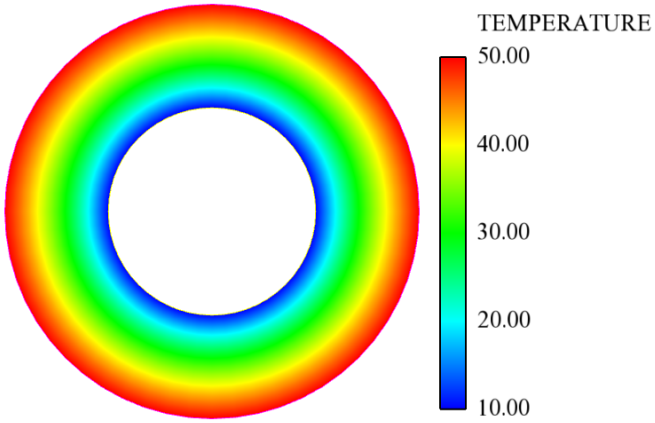

Figure 5.4: Converged thermal field

5.4.2 Comparison calculation results / analytical value

Comparisons between calculated values and analytical values are made along a radius of the ring.
Figure 5.5 presents a comparison between calculated and analytical profiles for calculation with the coarse mesh (on the left) and wity the fine mesh (on the right).

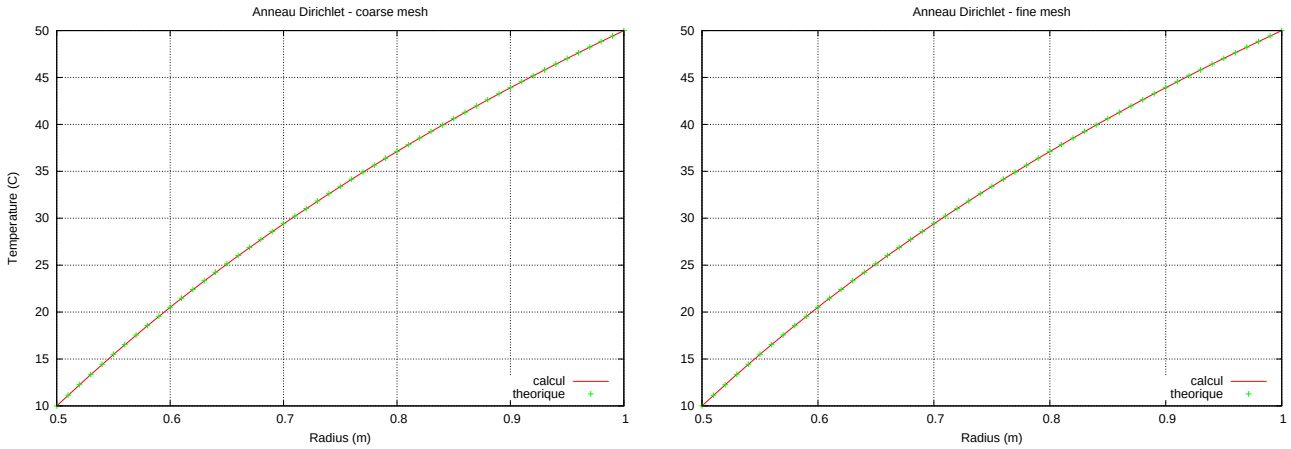

Figure 5.5: Theoretical profiles are calculated along a radius

Study of calculation's convergence
Following figures show evolution of temperature in 2 points given. Results are presented in the case of coarse and fine meshes. The two chosen nodes are :

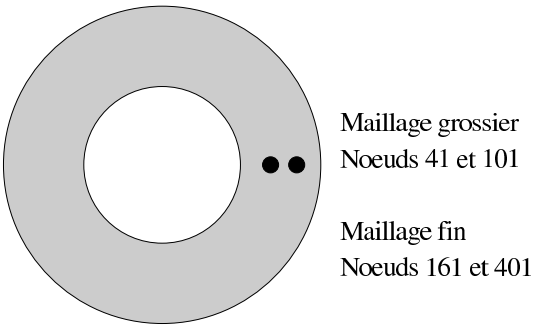

Figure 5.6: Positions of nodes for convergence study

Coarse mesh : used nodes's number

- Node 41 of coordinates $(0.61111, 0.)$
- Node 101 of coordinates $(0.77777, 0.)$

Fine mesh : used nodes's number

- Node 161 of coordinates $(0.60526, 0.)$
- Node 401 of coordinates $(0.76315, 0.)$

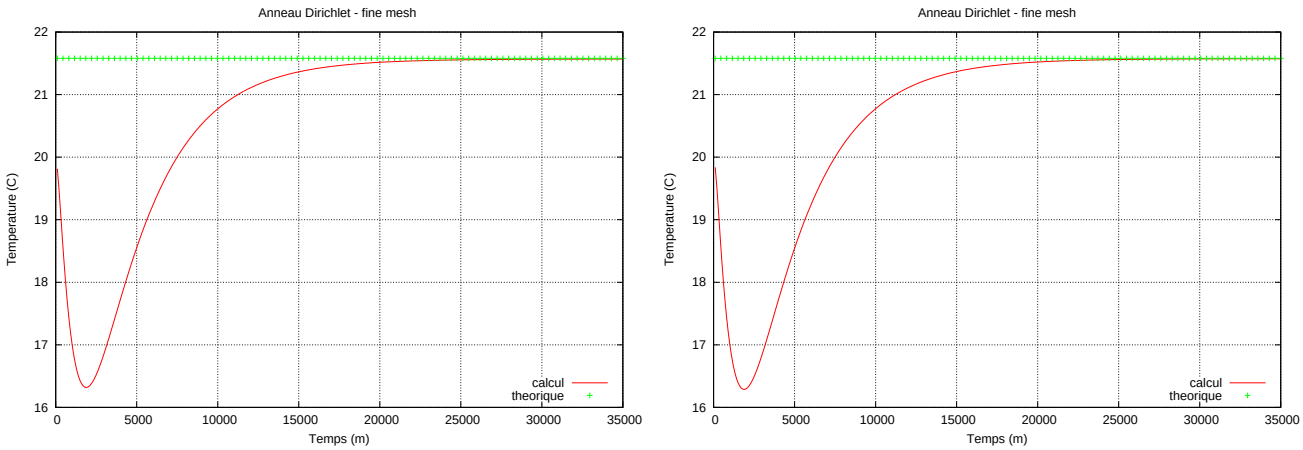

Figure 5.7: Study of convergence (Radius ≈ 0.61)

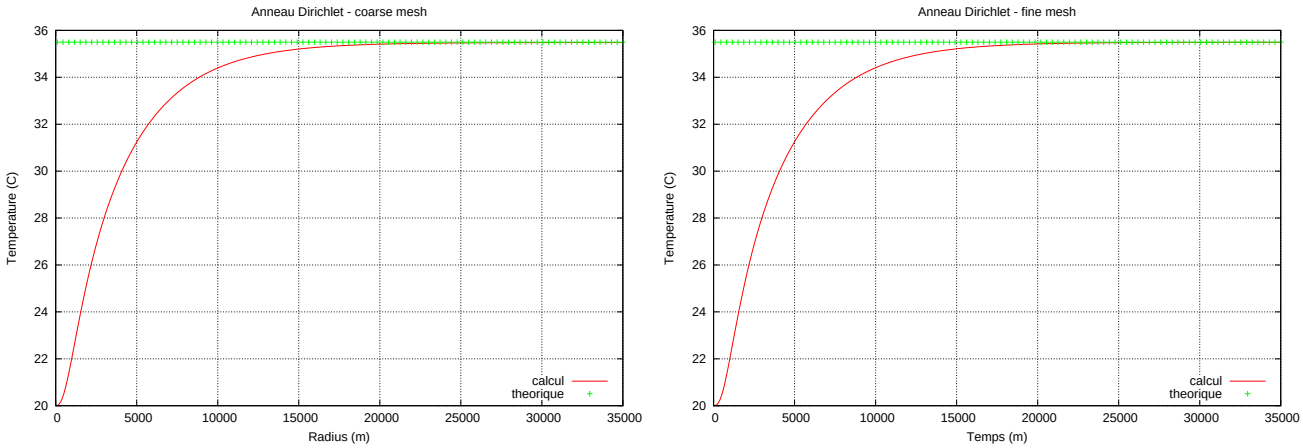

Figure 5.8: Study of convergence (Radius ≈ 0.77)

Remarks :
Like for previous configuration, error values mentionned on curves correspond to the absolute value of temperature gap between theoretical value and calculated value divided by the maximum observed temperature gap on the studied configuration.

5.5 Synthesis

The case ANNEAU gives satisfactory results. We find by calculation, the cylindrical nature of the solution (whereas elementary matrices are well understood cartesian).

Objective of this configuration is primarly to test the influence of mesh. The results confirm that calculated solution improves the mesh is refined.
In the present case, error's origin (which still remains low, a few thousandths to one hundredth degree on a temperature difference of about 40 $°C$) might arise from the fact that the spatial discretization implies faceting edges of cylinders. Perimeters on which we impose the boundary conditions are no longer strictly identical to the theoretical case. First approach, if we consider a perimete cut into n edge facets, the relative error committed on the perimeter is about :

$$\frac{\pi^2}{6n^2}\left[1-\frac{\pi^2}{20n^2}\right]$$

Similarly, error between the rope and the arc of the theoretical case may cause a position error about :

$$\frac{\pi^2}{n^2}\left[1-\frac{\pi^2}{24n^2}\right]$$

In the case of the ring, the numerical implementation with a cylinder cut in 76 facets give reltive errors about 2.84710^{-4} and 1.710^{-3} respectively for perimeter and positioning.

Chapter 6

ANNEAU-H

Features : Stationary 2D, boundary conditions of exchange coefficient type

Objectives : Validation of thermal resolution inside a 2D solid in a stationnary frame. Validation of boundary conditions's processing of exchange coefficient type.

6.1 Test case description

Geometry and physical conditions of this case are identical to those of test case "anneau". Only boundary conditions are different.

6.1.1 Geometry

We consider a ring whose inner radius is $R_a = 0.5\,m$ and outer radius is $R_b = 1\,m$.

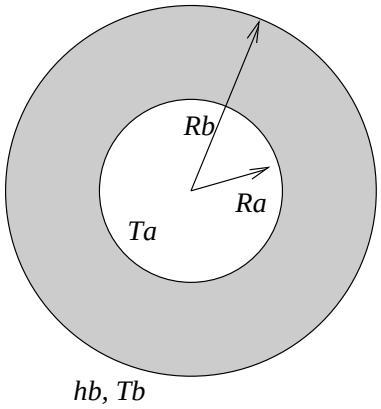

Figure 6.1: Solid domain

6.1.2 Physical conditions

The solid is related to steel having following physical characteristics:

- conductivity $k = 25\ W/mK$
- density $\rho = 7700\ kg/m^3$
- specific heat $C_p = 460\ J/kgK$

6.1.3 Initial conditions, boundary conditions

Initially (ï¿½ $t = 0$), the solid is at $20°C$.
We impose on the inside of the ring a temperature of $10°C$ and on the outside an exchange coefficient of $h = 10\ W/m^2K$ and an outside temperature of $50°C$.

6.2 Analitycal solution

In case of a small radius ring R_a and large radius R_b, which inside temperature is imposed at T_a and having on its external surface a exchange coefficient h_b and an external temperature T_b, we obtain at steady state the temperature at a point located at a radius r as follows :

$$T(r) = \frac{T_a \left(1 + h_b\ R_b\ \log\left(\frac{R_b}{r}\right)\right) + T_b\ h_b\ R_b\ \log\left(\frac{r}{R_a}\right)}{1 + h_b\ R_b\ \log\left(\frac{R_b}{R_a}\right)}$$

6.3 Calculations description

6.3.1 Mesh

The mesh (identical to the one of case “anneau” with coarse mesh) has :

- 2 888 ndes with 760 vertex nodes,
- 1 368 triangles.

Nodes of internal border have 1, those of the external border have reference 2, others have reference 0.

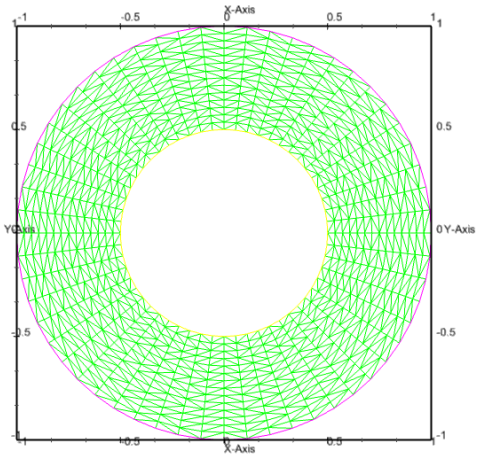

Figure 6.2: Mesh

6.4 Presentation of results

Steady state is obtained after nearly 1.5 days of physical time.

We have used a time step equal to 500 secondes.
Convergence has been reached after nearly 250 time steps.
Calculation needed 10.0 seconds on SGI station.

6.4.1 Thermal fields inside the ring

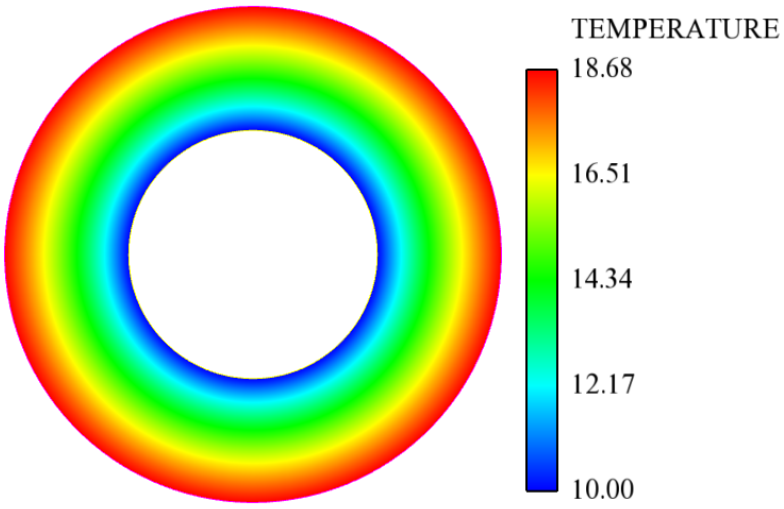

Figure 6.3: Converged thermal field

6.4.2 Comparison calculation results / analytical value

Comparisons between calculated values and analytical values (figure 6.4) are made along a radius of the ring.

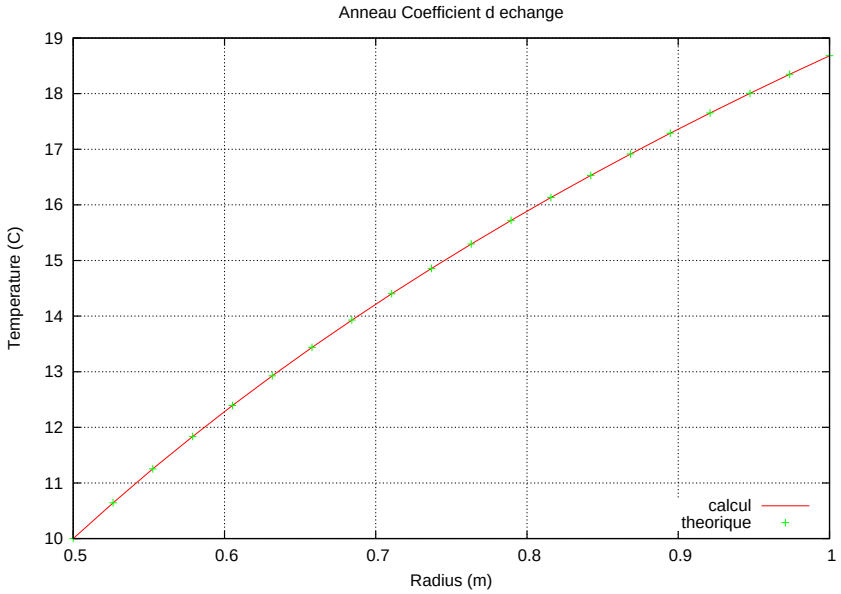

Figure 6.4: Theoretical profiles and calculated along a radius

Study of calculation's convergence

Figures 6.5 at 6.7 show the temperature's evolution in 3 points given :

- Node 41 of coordinates (0.611111)
- Node 101 of coordinates $(0.77777, 0.)$
- Node 181 of coordinates $(1., 0.)$

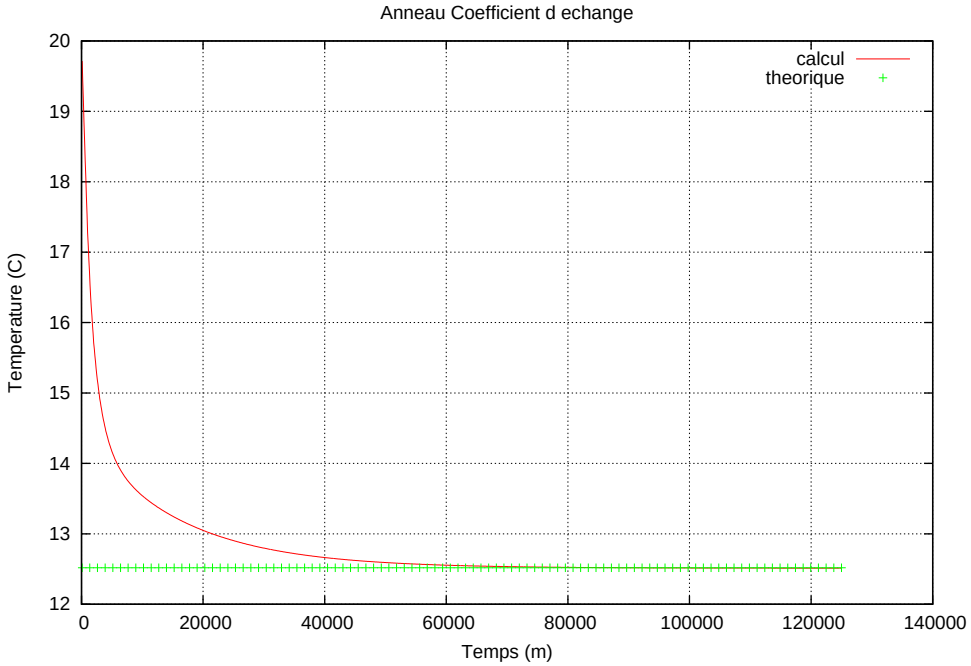

Figure 6.5: Convergence at R=0.611111

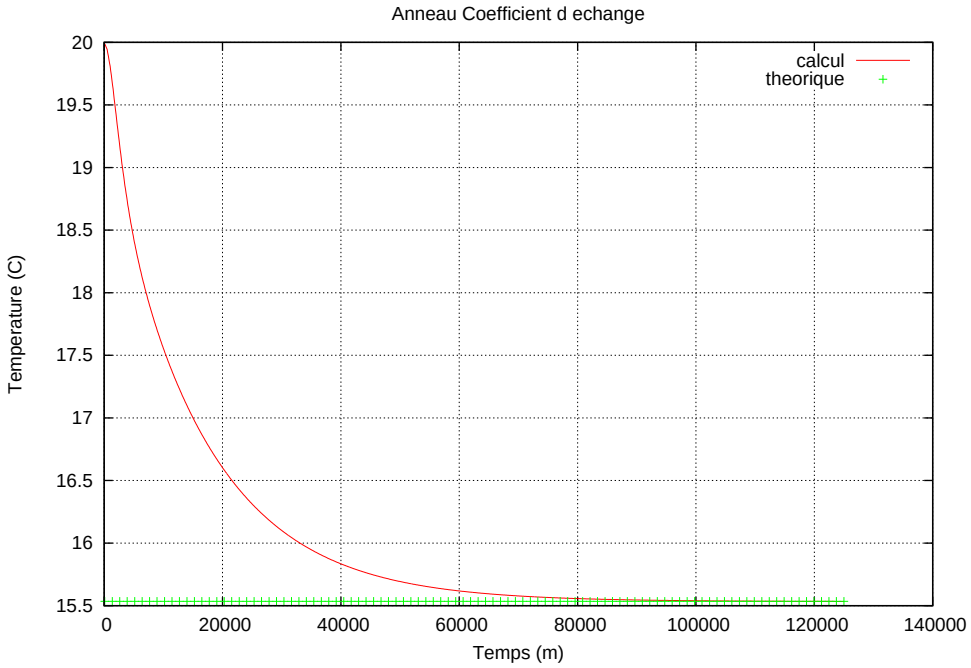

Figure 6.6: Convergence at R=0.77777

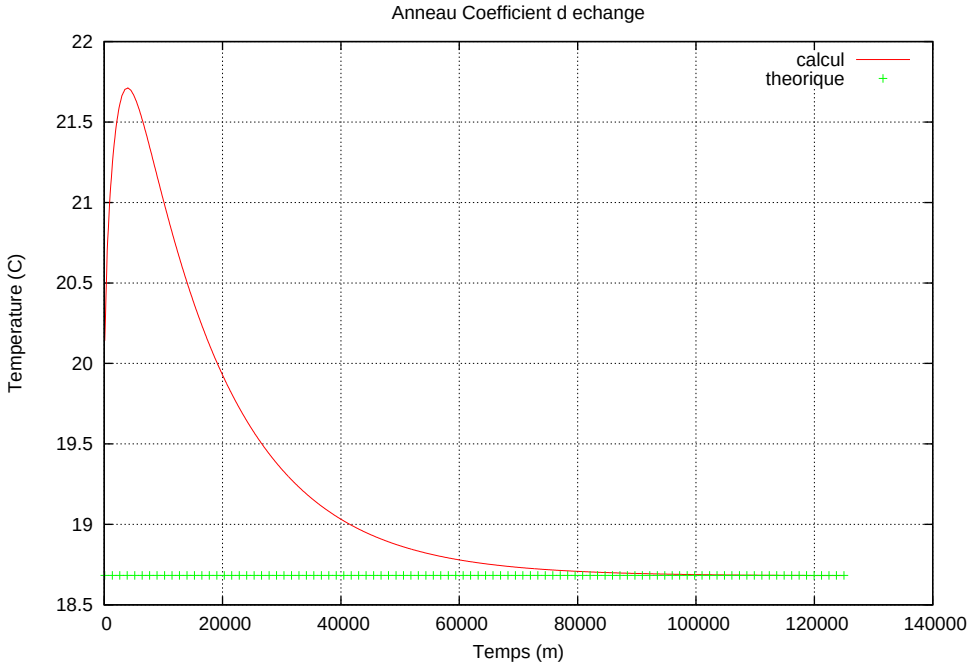

Figure 6.7: Convergence at R=1.

Remarks :
Like for previous configurations, error values mentionned on curves correspond to the absolute value of temperature gap between theoretical value and calculated value divided by the maximum observed temperature gap on the studied configuration.

6.5 Synthesis

Configuration ANNEAU-H is considered satisfactory. We could test in this configuration a case where conditions are only of exchange type, ie that temperatures at the border remain unknown values of the problem. The same remarks as the previous configuration may be done for faceting of geometry. it should however relativize this “approximation” relativiser cette “approximation” whose importance is still minimal. Indeed , be aware in an industrial configuration, the datasof problem (geometry, boundary conditions, materials behavior, etc...) are almost never known with the precesion level mentioned here.

Chapter 7

SPHERE

Characteristics : Unsteady 3D (here represened by a discrtization 2D), boundary conditions of Dirichlet type.

Objectives : Validation thermal resolution inside a solid in 2D in an unsteady frame. Validation of axisymmetric modeling. Validation of the treatment of Dirichlet's conditions.

7.1 Test case description

7.1.1 Geometry

We consider a solid sphere of radius : $R_a = 0.5m$

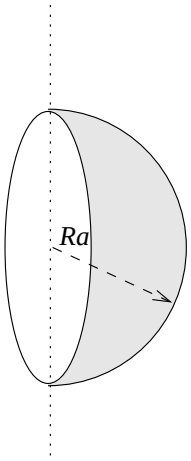

Figure 7.1: Solid domain

7.1.2 Physical conditions

The solid is related to steel having following physical characteristics :

- conductivity $k = 25\ W/mK$
- density $\rho = 7700kg/m^3$
- specific heat $C_p = 460J/kgK$

7.1.3 Initial conditions, boundary conditions

Initialy (at $t = 0$), the solid is at $0°C$.
We impose on the outer surface a temperature $T_a = 1°C$
In so far as the modeling is 2D axisymmetric, it must impose a boundary condition along the inside diameter of the sphere. A null flux condition will represent the 3D character of the case.

7.2 Analitycal solution

In the case of a sphere of radius R_a, we remind that the analitycal solution is written for a given radius r and t :

$$T(r) = T_a + \frac{2R_aT_a}{\pi r}\sum_{n=0}^{\infty}\frac{(-1)^n}{n}\ sin\left(\frac{n\pi r}{R_a}\right)\ e^{-\frac{kn^2\pi^2t}{{R_a}^2}}$$

A specific expression of this formula exist for the center of the sphere (obtained as limit $r \longrightarrow 0$ of the previous expression).

$$T(0) = T_a + 2T_a\sum_{n=1}^{\infty}(-1)^n\ \ e^{-\frac{kn^2\pi^2t}{{R_a}^2}}$$

7.3 Calculation description

7.3.1 Mesh

The mesh is realised in 2D, it uses axisymmetry property of the problem, this leads to mesh only a slice of sphere.

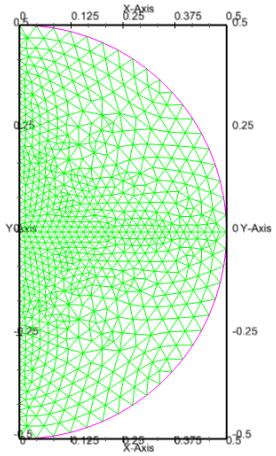

Figure 7.2: Mesh

The mesh has :

- 1 407 nodes with 369 vertex modes,
- 670 triangles.

The nodes of the sphere's diameter (x=0) have the reference 1, those of the outer border reference 2, others reference 0.

7.4 Presentation of results

We have performed calculation with a time step equal to 10 seconds, which allows to check the quality of prediction of thermal transient in an axisymmetric coordinate system.

Convergence has been reached after about 50000 physical seconds (about 14 hours), representing 5000 time steps.

The calculation has taken 31.2 seconds on SGI station.

7.4.1 Temperature field inside the sphere

From time $t = 0$, a progressive warming of the sphere appear. So expected isotherms are concentrically. We present here a hald section of the sphere after 1000, 2000, 5000 et 10000 seconds.

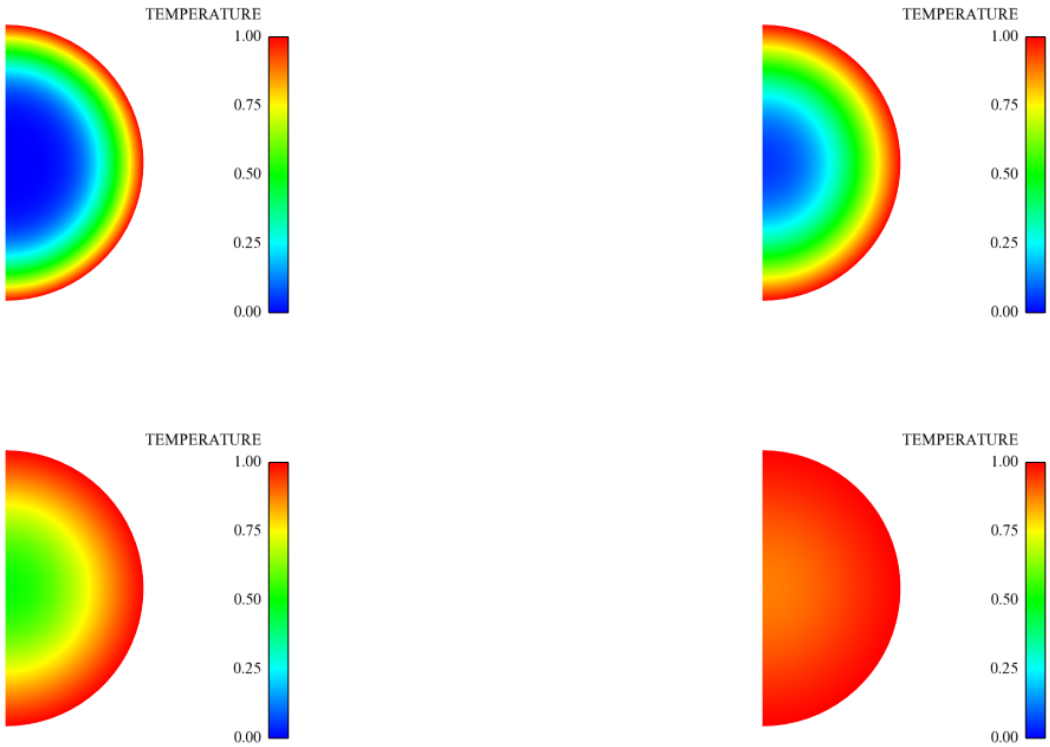

Figure 7.3: Temperature field at four moments

7.4.2 Comparison calculation results / analytical values

Comparisons between calculated values of temperature and analytical values aremade along a radius of the sphere at differents moments (100s, 1000s, 2500s, 5000s, 10000s, 20000s, 50000s). The analysed profile is defined as follows for the studied mesh :

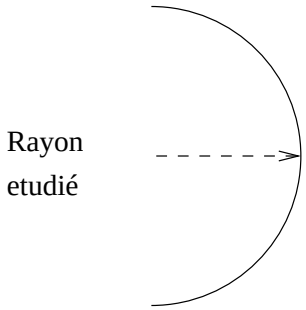

Figure 7.4: Profiles used for the results's evaluation

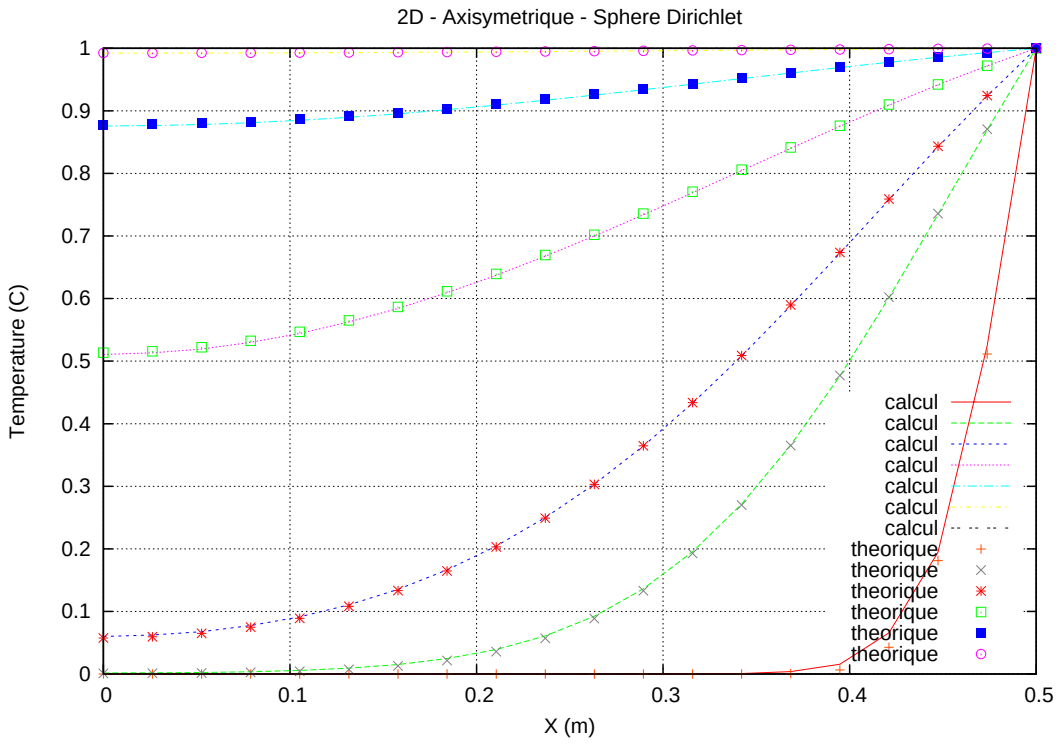

Figure 7.5: Theoretical profiles and calculated along a radius

Remarks :
On the first curve, we note a more angular profile. For plotting profiles only the values of vertex nodes are used and the plotter then connect the different values. Addition of middle nodes plot would already led to a more smoothed curve. Well use of a finer mesh would already led to obtain a curve closer to theoretical values.

Study of calculation's convergence

The figure 7.6 shows evolution of temperature at the center of the sphere. We note the good comparison of calculated transient with the theoretical transient.

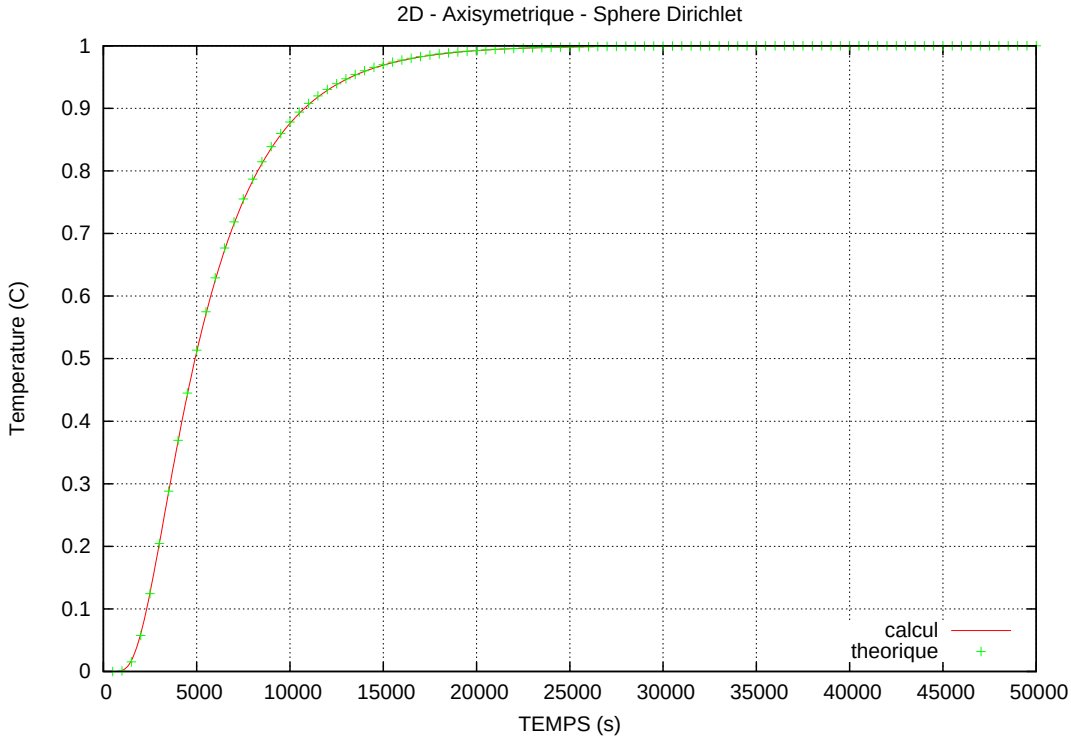

Figure 7.6: Study of the convergence in time

7.5 Synthesis

Results obtained with on the test case SPHERE are considered statisfactory. This test has particularly allowed to validate the construction of the elementary matrices for an axisymmetric coordinate system. The temperature field during transient is well concentric (corresponds well to the fact that this is a 1D problem in spherical coordinates). We also searched through this configuration to evaluate the quality of unsteady treatment done in SYRTHES. We see in figure 7.6 a good agreement between exact temporal to the center of the sphere and that obtained numeically. It should be noted that take a time step much higher lead to an error on evaluation of transient. If we interrested in more rigorous in the first instants of transient near the skin, where gradients are the most intense during transient, the mesh could be considered as insufficiently refined in this zone ,and the chosen time step high.

Chapter 8

BRIQUE

Characteristics : 3D, transient

Objectives : Validation of thermal resolution inside a solid for a 3D transient frame.

8.1 Test case description

8.1.1 Geometry

Consider a brik whose dimensions (in meters) are following :

- $-0.4 < x < 0.4$
- $-0.2 < y < 0.2$
- $-0.1 < z < 0.1$

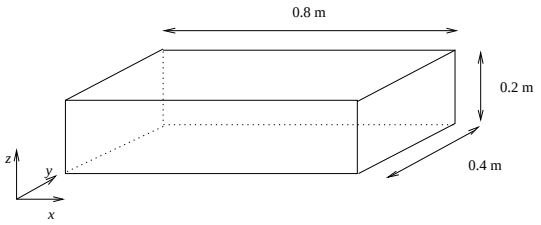

Figure 8.1: Calculation domain

8.1.2 Physical conditions

The solid is related to steel having following physical characteristics :

- conductivity $k = 25\ W/mK$
- density $\rho = 7700\ kg/m^3$
- specific heat $C_p = 460\ J/kgK$

8.1.3 Initial conditions, boundary conditions

Initially (at $t = 0$), the solid is at $0°C$.
We impose on the whole surface a temperature of $50°C$.

8.2 Analitycal solution

Consider a brick whose initial temperature is T_0 =0°C temperature on the surface is imposed at T_1=50°C and dimensions are :

- $-a < x < a$
- $-b < y < b$
- $-c < z < c$

Temperature inside the solid is given according to the instant t by the following analytical formula.

$$T = T_1 - \frac{64\ T_1}{\pi^3} \sum_{l=0}^{\infty} \sum_{n=0}^{\infty} \sum_{m=0}^{\infty} \frac{(-1)^{l+m+n}}{(2l+1)(2m+1)(2n+1)} cos\left(\frac{(2l+1)\pi x}{2a}\right) cos\left(\frac{(2m+1)\pi y}{2b}\right) cos\left(\frac{(2n+1)\pi z}{2c}\right) e^{-\alpha_{lmn} t}$$

avec

$$\alpha_{lmn} = \frac{k}{\rho C_p} \frac{\pi^2}{4} \left[\frac{(2l+1)^2}{a^2} + \frac{(2m+1)^2}{b^2} + \frac{(2n+1)^2}{c^2} \right]$$

8.3 Calculations description

8.3.1 Mesh

The mesh has :

- 102695 nodes with 13824 vertex nodes,
- 71346 tetrahedra.

Border nodes have reference 1 others, reference 0.

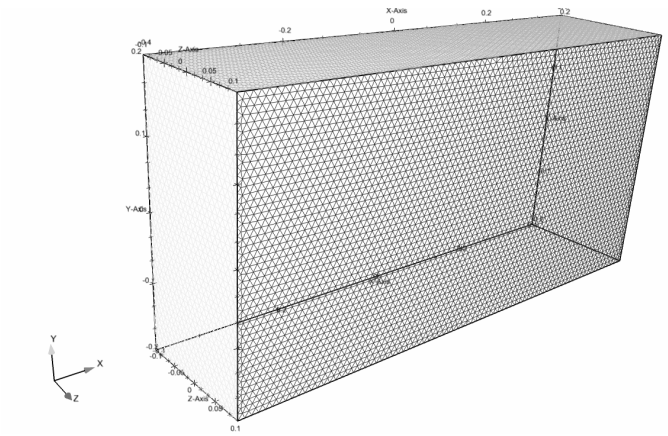

Figure 8.2: Mesh

8.4 Presentation of results

In so far we are interested to a transient phenomenon, the time step is 1 second in initial phase where temperature gradients are important then 10 s until convergence.

8.4.1 Thermal field inside the brick

Thermal field is presented at time t=1000 seconds.
Following the calculation temperature of the brick is of course constant and equal to $50°C$.

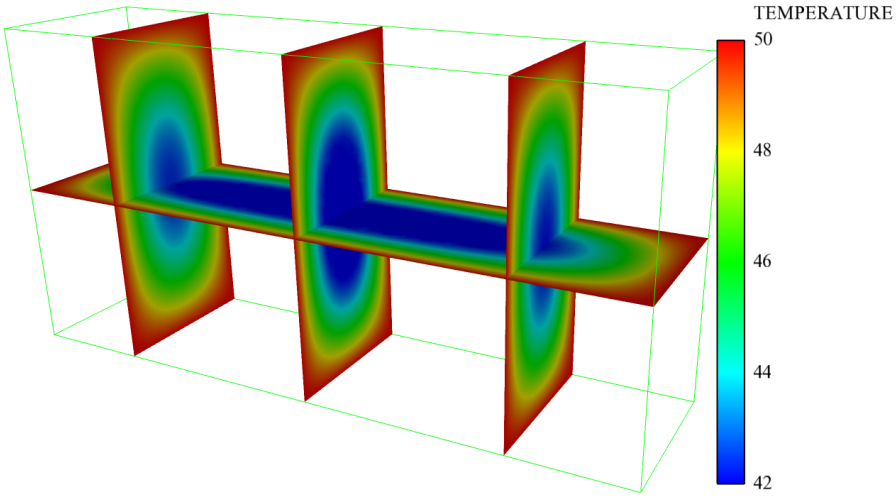

Figure 8.3: Thermal field at 1000 s

8.4.2 Comparison calculation results / analytical value

We present transient evolution of the temperature profile along a path y. Initialy only the points belonging to the edges of the brick are set to $50°C$, temperature in the other parts of the solid is closed to $0°C$. Then progressively, temperature in the center of the brick increases. After nearly 4000 seconds of real time, the temperature of the brick is $50°C$ at any point.

Following figures reprennent incorporate some of these profiles and compare them to theoretical profiles, obtained with the previously given analytical formula. For reasons of clarity, results are presented on 2 figures with separate scales, but note that the right one is the temporal continiuty of the left one (however scales have been adapted).

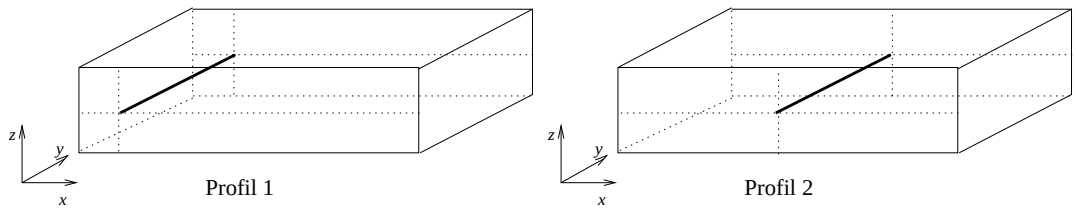

Figure 8.4: Position of the 2 studied profiles

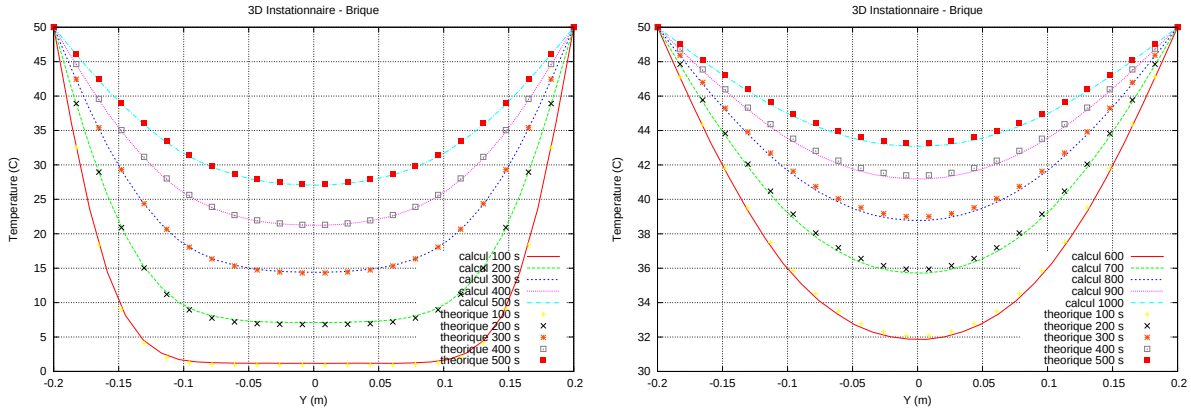

Figure 8.5: Profile 1 - Comparison calculation results / analytical values

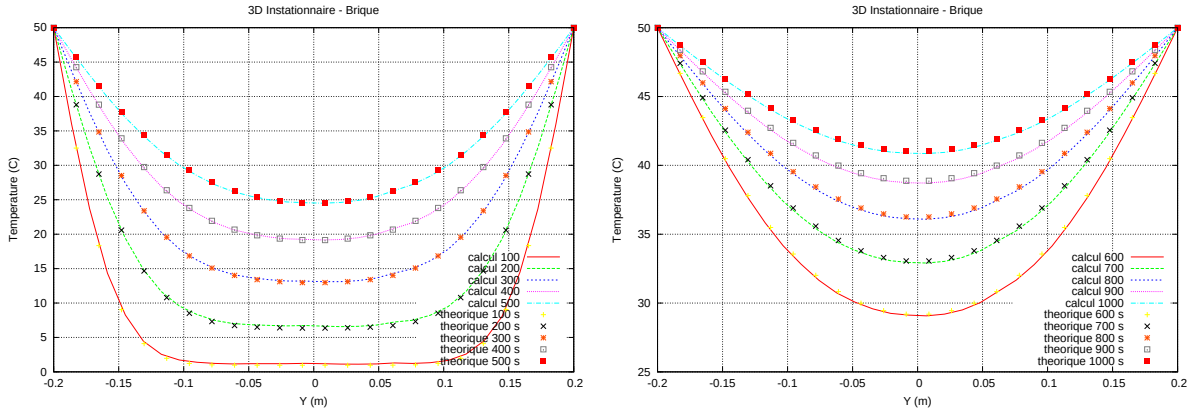

Figure 8.6: Profile 2 - Comparison calculation results / analytical values

Finally, we compare analytical values and calculated of temperature over time, in two given points :

- Node 7116 of coordinates $(-0.2683, -0.869\ 10^{-2}, -0.909\ 10^{-2})$
- Node 7500 of coordinates $(-0.8511\ 10^{-2}, -0.869\ 10^{-2}, -0.909\ 10^{-2})$

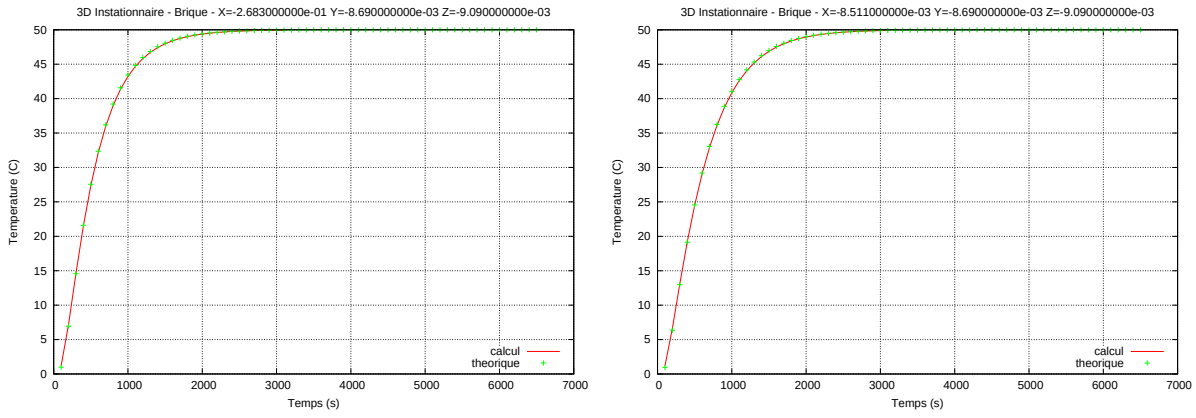

Figure 8.7: Thermal transient in 2 points

The comparison between calculated temperatures, and analytical solution is better for node 7500. This can be explained by the fact that this point closer to the center of the brick. Then, warming is more even.
To obtain such a good precision on the first point, a smaller value of of the time step would be better (the error is a function of time of δt).

8.5 Synthesis

Results obtained with the test case BRIQUE are considered satisfactory. This test case allowed, one hand, to validate construction of 3D elementary matrices, boundary conditions of Dirichlet in 3D, as consideration of transient aspect. It should be noted that this configuration is really 3D, in the sens that temperature gradients aren't aligned with any preferred axis. Like for some configurations already presented, it should be noted that in the case of industrial studies, it would be preferable to focus on mesh's refinement on the edges of the domain, where the temperature gradients seen during the transient are be the most important.

Part II

RAYONNEMENT

Chapter 9

Introduction

Le rayonnement constitue le deuxième mode de transfert d'énergie traité dans SYRTHES.
La notice théorique de SYRTHES [5] reprend en détail les aspects théoriques, les approximations retenues ainsi que les méthodes mises en œuvre pour le traitement du rayonnnement.

La méthode de radiosité retenue consiste à écrire un bilan énergétique sur chaque facette du domaine

$$J_i - \rho_i \sum_{j=1}^{n} F_{ij} J_j = M_i \quad \forall i$$

où J_i est la radiosité de la facette i, M_i l'émittance et ρ_i la réflectivité. F_{ij} qui est le facteur de forme entre les facettes i et j est une grandeur purement géométrique qui est constante au cours du calcul (si la géométrie ne change pas).
On rappelle que F_{ij}, intégrale quadruple, peut s'interpréter physiquement comme la proportion d'un éclairement partant de j qui atteint i.

En ce qui concerne le rayonnement, il convient donc de tester:

- la lecture des maillages surfaciques,
- le calcul des facteurs de forme (étape très importante pour la rigueur du calcul puisque cela conditionne la répartition d'énergie),
- la résolution du système radiatif,
- le couplage avec la conduction.

Les tests repris dans la suite du document soulignent la qualité des résultats obtenus dans ces diverses étapes.

Les premiers tests portent uniquement sur les calcul élémentaires de facteurs de forme. Même s'ils peuvent apparaître simples, ils sont parfaitement représentatifs des calculs effectués lors d'une étude industrielle. En effet, ils reprennent des configurations potentiellement rencontrées lors des calculs des facteurs de forme entre les couples de facettes composant le maillage.

On notera, concernant la dernière étape portant sur le couplage, que seules des configurations stationnaires ont été testées. La résolution numérique de cas instationnaire ne pose pas de difficultés et est immédiate (puisque par essence SYRTHES approche toujours les solutions de façon instationnaire) mais les solutions analytiques instationnaires qui correspondraient aux configurations (pourtant géométriquement simples) proposées dans ce document n'ont pu être

déterminées par les auteurs.
A ce propos, toute proposition de configurations couplant conduction et rayonnement admettant des solutions analytiques sera la bienvenue et pourra être intégrée dans une version ultérieure du document.

Chapter 10

Calcul des facteurs de forme

La validation du calcul des facteurs de forme a été réalisée sur des cas où des solutions analytiques existent [15],[6].
Par ailleurs, en milieu fermé, la somme des facteurs de forme d'une facette par rapport à toutes les autres doit être égale à 1. Cette propriété permet également une évaluation de la précision du calcul des facteurs de forme dans un domaine plus complexe.

10.1 Facteurs de forme en dimension 3

On présente ici trois cas :

- facteur de forme entre 2 facettes rectangulaires en vis-à-vis,
- facteur de forme entre 2 facettes jointives et faisant un angle θ,
- facteurs de forme dans un cylindre.

10.1.1 Cas de 2 facettes en vis-à-vis

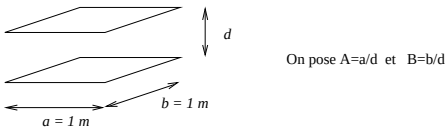

Figure 10.1: 2 facettes en vis-à-vis distantes de d

$$F_{12} = \frac{2}{\pi AB}\left[\log\sqrt{\frac{(1+A^2)(1+B^2)}{1+A^2+B^2}} + A\sqrt{1+B^2}\arctan\frac{A}{\sqrt{1+B^2}} + B\sqrt{1+A^2}\arctan\frac{B}{\sqrt{1+A^2}} - A\ \arctan\ A - B\ \arctan\ B\right]$$

Les résultats sont les suivants :

Distance d	Solution analytique	SYRTHES
10	0.00316205683	0.00316205683
1	0.19982489569	0.19982489569
0.1	0.82699452239	0.82699452297
0.01	0.98041660292	0.98041660542
0.001	0.99800563190	0.99800606681
0.0001	0.99980007097	0.99980026059

On remarquera que la précision est d'autant meilleure que la distance est importante. Cela provient du fait que la fonction à intégrer comporte le carré de l'inverse de la distance entre deux points parcourant chacune des facettes. Cette distance varie donc de façon beaucoup plus importante lorsque les deux facettes sont proches.

Remarque :
Il est à noter que ce cas est obtenu en redécoupant chaque facette en 2 triangles (seul type d'élément traité en 3D) puis en appliquant les règles d'additivité des facteurs de forme.

10.1.2 Cas de 2 facettes faisant un angle

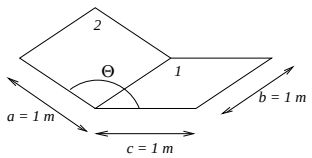

Figure 10.2: 2 facettes faisant un angle Θ

On pose

$$A = \frac{a}{b} \qquad B = \frac{c}{b} \qquad C = A^2 + B^2 - 2AB\cos\Theta$$

$$\begin{aligned}
F_{12}\pi B \;=\; & -\frac{\sin 2\Theta}{4}\left[AB\sin\Theta + (\frac{\pi}{2} - \Theta)(A^2 + B^2)\right. \\
& \qquad \left. + B^2\tan^{-1}\frac{A - B\cos\Theta}{B\sin\Theta} + A^2\tan^{-1}\frac{B - A\cos\Theta}{A\sin\Theta}\right] \\
& + \frac{\sin^2\Theta}{4}\left[(\frac{2}{sin^2\Theta} - 1)\log\frac{(1+A^2)(1+B^2)}{1+C}\right. \\
& \qquad \left. + B^2\log\frac{B^2(1+C)}{(1+B^2)C} + B^2\log\frac{A^2(1+A^2)^{\cos 2\Theta}}{C(1+C)^{\cos 2\Theta}}\right] \\
& + B\tan^{-1}\frac{1}{B} + A\tan^{-1}\frac{1}{A} - \sqrt{C}\tan^{-1}\frac{1}{\sqrt{C}} \\
& + \frac{\sin\Theta\sin 2\Theta}{2}\sqrt{1 + A^2\sin^2\Theta} \\
& \qquad \left[\tan^{-1}\frac{A\cos\Theta}{\sqrt{1 + A^2\sin^2\Theta}} + \tan^{-1}\frac{B - A\cos\Theta}{\sqrt{1 + A^2\sin^2\Theta}}\right] \\
& + \cos\Theta\int_0^B \sqrt{1 + \xi^2\sin^2\Theta} \\
& \qquad \left(\tan^{-1}\frac{A - \xi\cos\Theta}{\sqrt{1 + \xi^2\sin^2\Theta}} + \tan^{-1}\frac{\xi\cos\Theta}{\sqrt{1 + \xi^2\sin^2\Theta}}\right) d\xi
\end{aligned}$$

On remarquera que cette configuration a la particularité de posséder des facettes ayant une arête commune. Mathématiquement cela signifie que la fonction à intégrer devient singulière (puisqu'elle fait intervenir la distance entre les points des arêtes).
Cependant, l'intégrale de cette fonction singulière reste bornée (l'énergie restant finie).

Les résultats sont les suivants :

Angle θ	Analytique	SYRTHES
30	0.619028	0.61902831
60	0.370905	0.37090532
90	0.200044	0.20004377
120	0.086615	0.08661500
150	0.021346	0.02134532
180	0.	0.00000002

10.1.3 Facteurs de forme dans un cylindre

On présente ci-dessous le maillage surfacique du cylindre qui a été utilisé pour le calcul des facteurs de forme (1064 facettes).

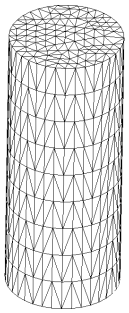

Figure 10.3: Maillage pour le calcul des facteurs de forme

On rappelle que l'on doit vérifier : $\sum_{j=1}^{N} F_{ij} = 1$ (cette relation découle de la conservation de l'énergie).

La figure suivante présente les valeurs de la somme des facteurs de forme pour chacune des facettes du maillage. On peut remarquer que l'erreur maximale sur la somme est de l'ordre de 10^{-6}.

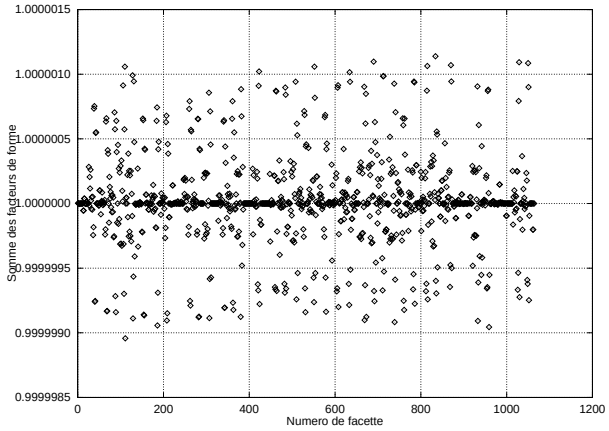

Figure 10.4: Somme des facteurs de forme

Remarque :
En toute rigueur, ce test permet de s'assurer que l'énergie est bien conservée mais pas d'affirmer que chacun des facteurs de forme est calculé de façon aussi précise.

10.2 Facteurs de forme en axisymétrique

10.2.1 Cas de 2 anneaux sur un cylindre

On souhaite calculer le facteur de forme entre deux anneaux définis sur un cylindre de rayon r. Le calcul est réalisé en axisymétrique. Au niveau de SYRTHES, le maillage nécessaire pour le calcul se réduit ainsi à deux segments verticaux.
Le cas est présenté sur la figure 10.5 :

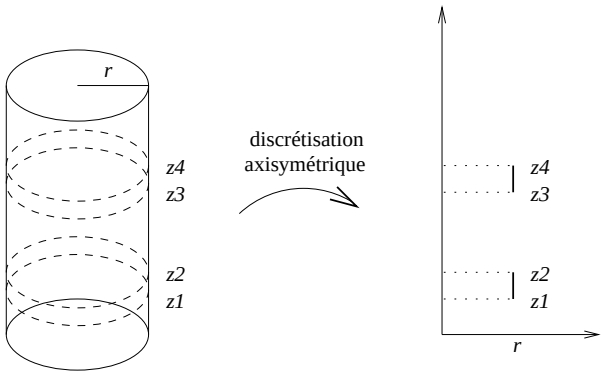

Figure 10.5: 2 anneaux sur un cylindre - calcul en axisymétrique

La surface 1 est définie par l'anneau $z_1 - z_2$ et la surface 2 par l'anneau $z_3 - z_4$.
L'expression du facteur de forme est donnée par

$$F_{12} = \frac{1}{4r(z_2 - z_1)} \left[f(z_2 - z_3) - f(z_2 - z_4) + f(z_1 - z_4) - f(z_1 - z_3) \right]$$

avec

$$f(x) = x^2 - |x|\sqrt{x^2 + 4r^2} + 2r|x|$$

Pour une telle configuration, tous les points du premier anneau voient tous les points du second. Le cas a été étudié pour diverses configurations en faisant varier d'une part l'épaisseur de l'anneau supérieur et d'autre part la distance entre les deux anneaux.
Les résultats sont présentés dans le tableau ci-dessous. On notera une très bonne précision des résultats fournis par SYRTHES.

r	z1	z2	z3	z4	Analytique	Calcul numérique
1	0	0.1	1.	1.1	0.0187129268378	0.018712926838
1	0	0.1	0.5	0.6	0.0321822739118	0.032182273911
1	0	0.1	0.11	0.21	0.0458896098695	0.045889609869
1	0	0.1	0.1	0.2	0.0462616576130	0.046261657613
1	0	0.1	0.2	0.7	0.1782713873497	0.178271362840

10.2.2 Cas de 2 anneaux sur un tronc de cône

On souhaite calculer le facteur de forme entre deux anneaux définis sur un tronc de cône. Ce dernier est caractérisé par le rayon de sa base r et son ouverture ψ. Le calcul est réalisé en axisymétrique. Au niveau de SYRTHES, le maillage nécessaire pour le calcul se réduit ainsi à deux segments inclinés.
Le cas est présenté sur la figure 10.6 :

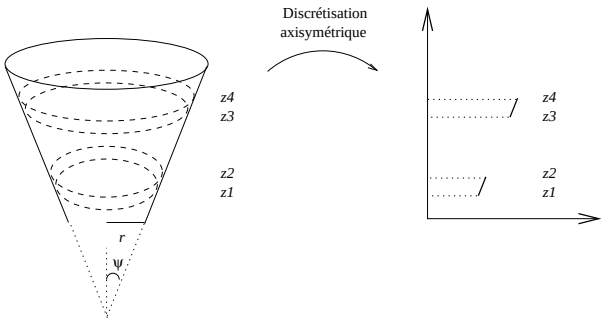

Figure 10.6: 2 anneaux sur un cône - calcul en axisymétrique

La surface 1 est définie par l'anneau $z_1 - z_2$ et la surface 2 par l'anneau $z_3 - z_4$.

L'expression du facteur de forme est donnée par

$$F_{12} = \frac{\frac{1}{2}\sin\psi}{2r(z_2 - z_1) + \frac{{z_2}^2 - {z_1}^2}{\tan\psi}} \times [2(z_2 - z_1)(z_4 - z_3) + f(z_2, z_4) - f(z_1, z_4) + f(z_1, z_3) - f(z_2, z_3)]$$

avec

$$f(x,y) = \sqrt{\left[(x-y)^2 + \left(r + \frac{x}{\tan\psi}\right)^2 + \left(r + \frac{y}{\tan\psi}\right)^2\right]^2 - \left[2\left(r + \frac{x}{\tan\psi}\right)\left(r + \frac{y}{\tan\psi}\right)\right]^2}$$

Le calcul a été réalisé pour deux angles d'ouverture et dans chaque cas, pour deux épaisseurs d'anneaux différentes.
Les résultats sont présentés dans le tableau ci-dessous. On notera une très bonne précision des résultats fournis par SYRTHES.

r	ψ	$z1$	$z2$	$z3$	$z4$	Analytique	Calcul numérique
0.5	$\pi/6$	0.	0.1	0.5	0.6	0.0145100568276	0.014510056830
0.5	$\pi/6$	0.	0.1	0.2	0.25	0.0139078991326	0.013907899019
0.5	$\pi/4$	0.	0.1	0.5	0.6	0.0260748111926	0.026074811215
0.5	$\pi/4$	0.	0.1	0.2	0.25	0.0229771224013	0.022977122422

10.2.3 Cas d'un anneau sur un cône, l'autre sur un cylindre

On souhaite calculer le facteur de forme entre deux anneaux, le premier étant défini sur un tronc de cône, le second sur un cylindre. Le tronc de cône est caractérisé par le rayon de sa base r_1 et son ouverture ψ, le cylindre a un rayon r_2. Le calcul est réalisé en axisymétrique. Au niveau de SYRTHES, le maillage nécessaire pour le calcul se réduit ainsi à deux segments, l'un vertical, l'autre incliné.
Le cas est présenté sur la figure 10.7 :

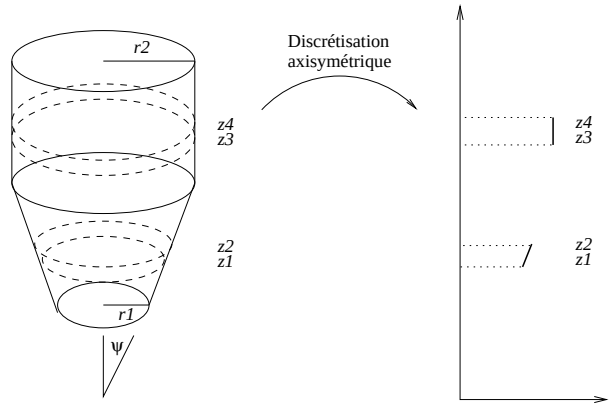

Figure 10.7: Anneaux sur un cône et un cylindre - calcul en axisymétrique

L'expression du facteur de forme est donnée par

$$\begin{aligned} F_{12} &= \frac{\frac{1}{2}\,\sin\psi}{2r_1(z_2-z_1)+\frac{{z_2}^2-{z_1}^2}{\tan\psi}} \times \\ &\quad [2(z_2-z_1)(z_4-z_3)+f(z_3,z_1)-f(z_3,z_2)+f(z_4,z_2)-f(z_4,z_1)] \end{aligned}$$

avec

$$f(x,y)=\sqrt{\left[(x-y)^2+{r_2}^2+\left(r_1+\frac{y}{\tan\psi}\right)^2\right]^2-\left[2r_2\left(r_1+\frac{y}{\tan\psi}\right)\right]^2}$$

Le calcul a été réalisé pour deux angles d'ouverture et dans chaque cas, pour deux épaisseurs d'anneaux différentes.
Les résultats sont présentés dans le tableau ci-dessous. On notera une très bonne précision des résultats fournis par SYRTHES.

$r1$	$r2$	ψ	$z1$	$z2$	$z3$	$z4$	Analytique	Calcul numérique
0.5	1.	$\pi/6$	0.	0.1	0.5	0.6	0.0655544734077	0.065554508966
0.5	1.	$\pi/4$	0.	0.1	0.5	0.6	0.0535358509414	0.053535849698
0.5	1.	$\pi/6$	0.	0.1	0.12	0.7	0.2821714144798	0.281463904352
0.5	1.	$\pi/4$	0.	0.1	0.12	0.7	0.1838728520392	0.183610892562

10.2.4 Cas de 2 anneaux en vis-à-vis

On souhaite calculer le facteur de forme entre deux anneaux en vis-à-vis. Les anneaux sont caractérisés par leurs rayons. Le calcul est réalisé en axisymétrique. Au niveau de SYRTHES, le maillage nécessaire pour le calcul se réduit ainsi à deux segments horizontaux.
Le cas est présenté sur la figure 10.8 :

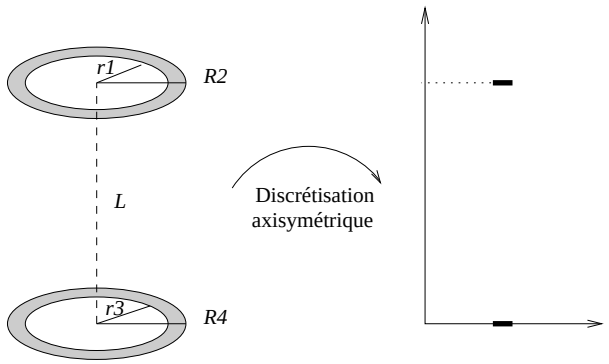

Figure 10.8: Anneaux en vis-à-vis - calcul en axisymétrique

$$F_{12} = \frac{1}{2}\left[\frac{{R_4}^2 - {r_3}^2}{{r_1}^2} - \sqrt{\left(1 + \frac{{R_4}^2 + L^2}{{r_1}^2}\right)^2 - 4\frac{{R_4}^2}{{r_1}^2}} + \sqrt{\left(1 + \frac{{r_3}^2 + L^2}{{r_1}^2}\right)^2 - 4\frac{{r_3}^2}{{r_1}^2}}\right]$$

Le calcul a été réalisé pour plusieurs valeurs de la distance L entre les deux anneaux.
Les résultats sont présentés dans le tableau ci-dessous.

$r1$	$R2$	$r3$	$R4$	L	Analytique	Calcul numérique
0.5	0.6	0.5	0.6	1.	0.0535424552602	0.053542455350
0.5	0.6	0.5	0.6	0.5	0.1055306803864	0.105530689990
0.5	0.6	0.5	0.6	0.1	0.4158876592597	0.415941427592

On remarque, comme dans le cas des deux plans se faisant face, que l'estimation numérique des facteurs de forme est d'autant meilleure que les deux disques sont éloignés. La raison est en la même.

10.2.5 Traitement des faces cachées : disque perpendiculaire à un cylindre

On s'intéresse maintenant aux configurations qui font intervenir les calculs d'ombrage dans la détermination des facteurs de forme en axisymétrique.

Le cas est présenté ci dessous. Il s'agit du calcul du facteur de forme entre un disque D et un cylindre C.

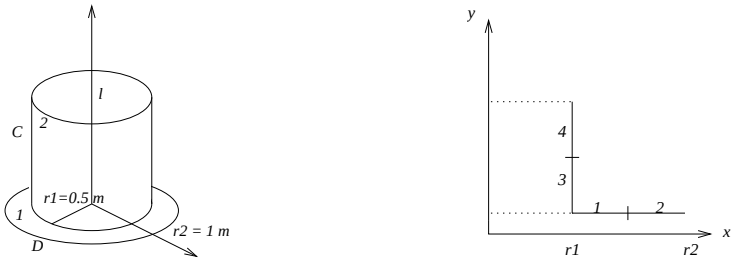

Figure 10.9: Cas d'un disque perpendiculaire à un cylindre

On pose

$$R = \frac{r_2}{r_1} \qquad L = \frac{l}{r_1}$$

Alors, on a

$$\begin{aligned} F_{12} \;=\; & \frac{1}{\pi(1-R^2)} \left[(1-R^2)\tan^{-1}\sqrt{\frac{1+R}{1-R}} \right. \\ & -\sqrt{(1+R^2+L^2)^2-4R^2}\,\tan^{-1}\sqrt{\frac{(1+R^2+L^2+2R)(1-R)}{(1+R^2+L^2-2R)(1+R)}} \\ & \left. +\frac{1}{2}L^2\cos^{-1}R + 2RL\tan^{-1}\frac{\sqrt{1-R^2}}{L} \right]. \end{aligned}$$

Sur la base de ce cas-test, nous allons considérer 4 facettes. Les deux premières sont sur le disque D (facettes 1 et 2) , les 2 suivantes sur le cylindre C (facettes 3 et 4).

Ces tests font intervenir le calcul des surfaces cachées. Lorsqu'un ombrage est détecté, il est possible de demander au code un redécoupage automatique des facettes pour obtenir localement une meilleure discrétisation de la géométrie. Dans le cas des segments, le premier redécoupage conduit à considérer 2 sous-segments. Lorsque l'on demande 2 redécoupages, on considèrera au final les 4 sous-segments qui constituent chaque segment.

Le tableau ci-dessous indique les valeurs de la surface multipliée par le facteur de forme pour un couple de facettes. On présente également les résultats avec 1 et 2 redécoupages des facettes.

Surf x Facteur de forme	S_4F_{41}	S_3F_{32}
Analytique	0.0827264975	0.2155427154
0 redécoupage	0.08259126	0.21264747
1 redécoupage	0.08267165	0.21389134
2 redécoupages	0.08270403	0.21463669

Remarque :
On peut noter que le facteur de forme S_4F_{41} est mieux estimé que S_3F_{32}. Il est éventuellement

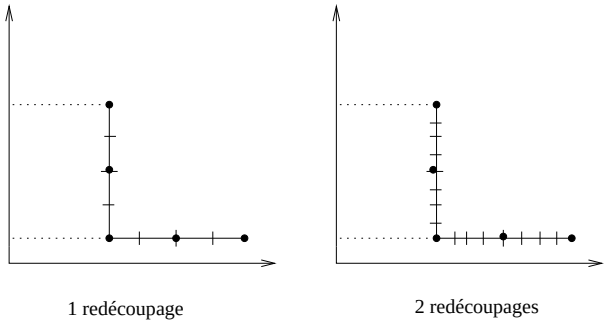

Figure 10.10: Redécoupage des facettes

envisageable que la discrétisation angulaire ait plus d'importance pour des facettes plus éloignées. Cependant, une étude plus approfondie serait nécessaire pour fournir une explication rigoureuse de cette différence.

10.2.6 Traitement des faces cachées : deux cylindres concentriques

Le cas est présenté sur la figure suivante

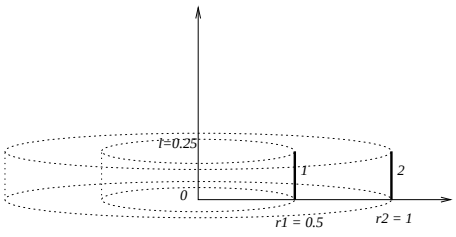

Figure 10.11: Cas de deux cylindres concentriques

On pose

$$\begin{aligned} R &= \frac{r_2}{r_1} \\ L &= \frac{l}{r_1} \end{aligned}$$

Alors, on a

$$\begin{aligned} F_{12} &= \frac{1}{R} - \frac{1}{\pi R}\left\{\cos^{-1}\frac{B}{A}\right. \\ &\quad \left. -\frac{1}{2L}\left[\sqrt{(A+2)^2-4R^2}\cos^{-1}\frac{B}{RA} + B\sin^{-1}\frac{1}{R}\frac{\pi A}{2}\right]\right\} \end{aligned}$$

Le tableau ci-dessous indique les valeurs de la surface multipliée par le facteur de forme les deux facettes. Come dans le cas 10.2.5, on présente également les résultats avec 1 et 2 redécouplages des facettes.

Surf x Facteur de forme	S_1F_{12}
Analytique	0.21094110
0 redécoupage	0.21094158
1 redécoupage	0.21094158
2 redécoupages	0.21094158

Remarque :
On remarque que sur ce cas précis le fait de redécouper n'entraine pas d'amélioration du résultat. L'explication réside dans le fait que, sur cet exemple, la position angulaire correspondant au masquage provoqué par la facette 1 (cylindre intérieur) correspond à un même angle limite que les segments soient redécoupés ou non. Cela ne serait plus vrai s'il existait un obstacle intermédiaire.

Un cas similaire a été testé en rapprochant les 2 cylindres.

Surf x Facteur de forme	S_1F_{12}
Analytique	1.2384039767
0 redécoupage	1.23842909
1 redécoupage	1.23842908

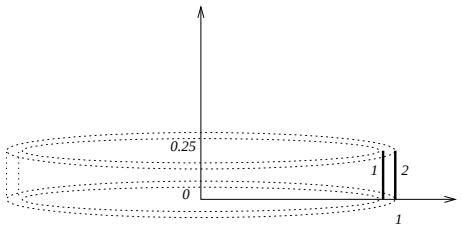

Figure 10.12: Cas de deux cylindres concentriques à courte distance

Remarque :
Comme pour le cas précédent, le redécoupage n'apporte pas d'amélioration et la même remarque concernant les angles limites s'applique.

10.2.7 Traitement des faces cachées : cône et disque

On considère 2 facettes sur un cône à 45° et 2 autres sur un disque. Le cas est présenté sur la figure suivante

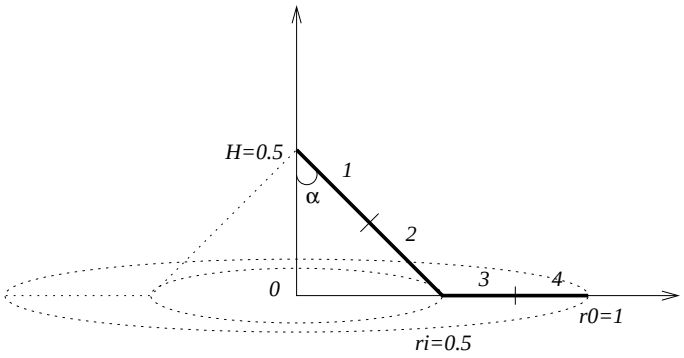

Figure 10.13: Cas de facettes sur un cône et un disque

Les formules analytiques existent, mais deviennent fort complexes. Si on pose $R_i = r_i/r_o$, et les termes auxiliaires

$$A = \sqrt{H^2 + (1 + H\tan\alpha + R_i)^2}$$
$$B = \sqrt{H^2 + (1 - H\tan\alpha - R_i)^2}$$
$$C = \sqrt{1 - {R_i}^2}$$
$$D = \sqrt{1 + {R_i}^2}$$
$$E = \cos^2\alpha(1 - {R_i}^2)$$

on a

$$F_{41} = \frac{1}{\pi(1-{R_i}^2)}\left\{-AB\tan^{-1}\frac{AB}{CD} + C^2D^2\tan^{-1}\frac{D}{C}\right.$$
$$+\frac{\sin\alpha}{\cos^2\alpha}\left[\left(H^2 + \frac{2HR_i}{\tan\alpha}\right)\tan^{-1}\frac{\sqrt{E}}{H} + E\tan^{-1}\frac{H}{\sqrt{E}}\right]$$
$$\left.+\left(\frac{H^2}{2\cos^2\alpha} + HR_i\tan\alpha\right)\cos^{-1}R_i\right\}$$

Le tableau ci-dessous indique les valeurs de la surface multipliée par le facteur de forme pour le couple de facettes 4-1.
Come dans le cas 10.2.5, on présente également les résultats avec 1 et 2 redécouplages des facettes.

Surf x Facteur de forme	S_4F_{41}
Analytique	0.00530000448
0 redécoupage	0.00527607
1 redécoupage	0.00528986
2 redécoupages	0.00529548

Remarque :
Contrairement aux configurations précédentes, on note sur ce cas une amélioration du facteur de forme avec le nombre de redécoupages. Cela est dû au fait qu'avec un redécoupage, on estime mieux chaque sous-segment.

10.3 Synthèse de la validation des facteurs de forme

On a vu dans les paragraphes précédents que les facteurs de forme (quantité purement géométrique) sont estimés de façon rigoureuse dans SYRTHES, au moins dans le cas de configurations simples pour lesquelles des solutions analytiques existent.
Cela ne signifie pas que toutes les situations rencontrées dans les cas industriels seront calculées avec ce niveau de précision. En effet, les effets d'ombrage sont particulièrement difficiles à prendre en compte et l'on manque de configurations de référence.

C'est pourquoi les auteurs insistent sur l'importance que peut avoir la réalisation du maillage de rayonnement sur la qualité des résultats. Il convient en particulier d'utiliser des éléments dont la taille est en rapport avec le problème physique que l'on souhaite traiter (pas trop grands dans les zones a forts gradients, dans les zones d'ombrages, etc...). En effet, on rappelle que, d'une part, la température est supposée constante par facette (méthode de radiosité) et que d'autre part, des éléments de taille non adaptée pourraient induire des erreurs sur l'influence des facette occultrices.

Nous venons également de montrer que le redécoupage automatique des facettes pouvait améliorer le calcul des facteurs de forme. Il faut toutefois garder à l'esprit qu'il reste préférable d'utiliser un maillage adapté (suffisamment fin aux endroits délicats). En effet, si le redécoupage permet d'augmenter la précision des facteurs de forme, la température n'en reste pas moins constante par facette. Par ailleurs, le redécoupage est une option qui entraine un surcoût important : un facteur 4 pour 1 redécoupage, un facteur 16 pour 2 redécoupages, etc... Même si ces données géométriques ne sont calculées qu'une fois par calcul, le coût CPU peut être non négligeable. Les procédures de calcul utilisées devraient cependant limiter le coût CPU à des valeurs raisonnables.

Chapter 11

Validation du solveur

Les cas-tests précédents ont permis d'apprécier la qualité du calcul des facteurs de forme. Il convient également de bien valider le solveur pour la résolution du système de rayonnement.

On considère un cylindre de hauteur L et de rayon R.
La température du milieu ambiant (T_e) est fixée à 0, la température du pourtour du cylindre et de sa base est fixée à T_w, on calcule le flux radiatif Q passant à travers la face supérieure du cylindre.

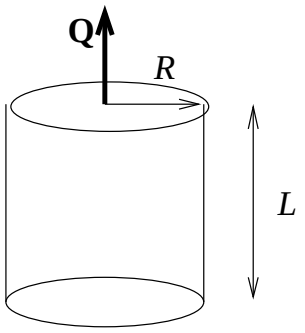

Figure 11.1: Domaine de calcul

A partir de ces grandeurs, on peut construire une émissivité équivalente :

$$\varepsilon = \frac{Q}{\pi R^2 \sigma (T_w^4 - T_e^4)}$$

Le cas-test est réalisé pour plusieurs valeurs du rapport L/R.

Les maillages utilisés pour les différents rapports de L/R sont les suivants :

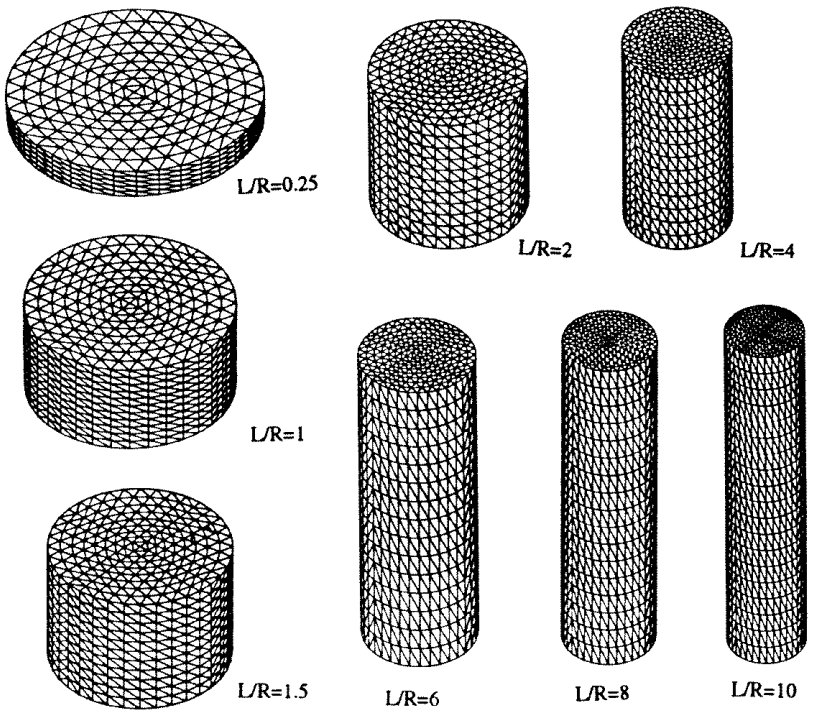

Figure 11.2: Les différents maillages utilisés

La section de tous les cylindres est discrétisée de façon identique. Elle comporte 324 éléments. Les nombre de sections verticales sont reprises dans le tableau suivant

L/R	0.25	1	1.5	2	4	6	8	10
Sections	6	12	12	12	14	16	18	20

On trace ensuite la valeur du flux pour les différents ratios L/R et pour différentes valeurs de l'émissivité ε (les losanges indiquent les valeurs analytiques). Les valeurs analytiques sont issues de la littérature.

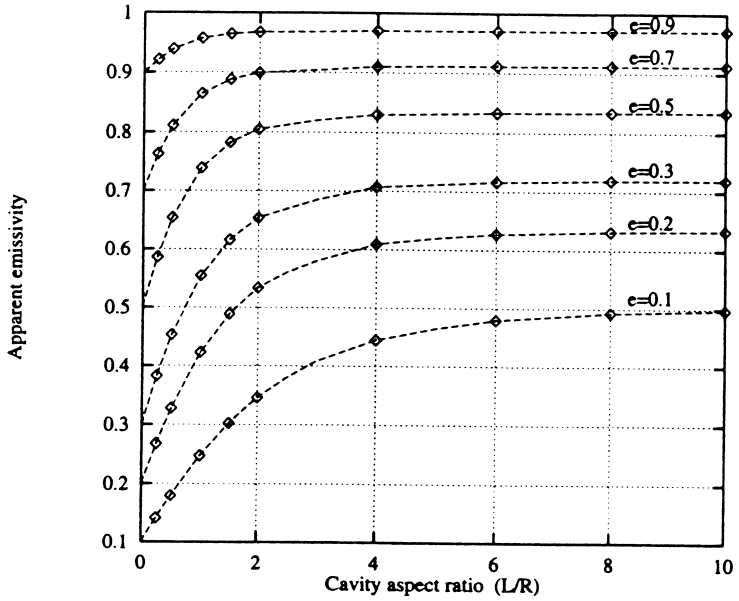

Le bon accord entre les résultats numériques et les valeurs de référence montrent :

- que les facteurs de forme ont été évalués correctement, ce qui n'est pas surprenant au vu des tests effectués sur les configurations élémentaires et sur le cylindre présenté au paragraphe 10.1.3,
- que les radiosités sont évaluées correctement. Cela indique donc une résolution rigoureuse du système radiatif.

Chapter 12

COND_RAY

Characteristics : Stationnary 2D cartesian, coupling conduction/radiation.

Objectives : Validation of radiative calculation in 2D cartesian and validation of coupling conduction/radiation.

12.1 Test case description

12.1.1 Geometry

Consider a channel of infinite length in order to be able to assume that thermal transfers are 1D inside a slice. This permits to compare calculation results to a analytical solution.

In practice, we define a channel one meter long and 3 cm wide. Walls's thickness is 1 cm.

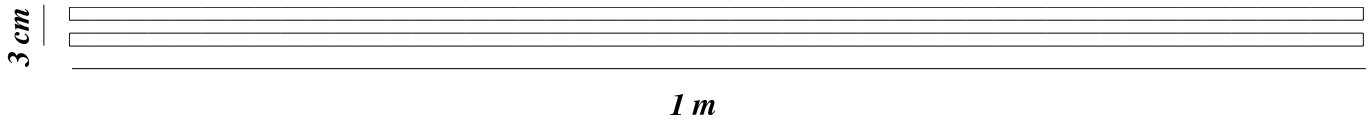

Figure 12.1: Solid domain

12.1.2 Physical conditions

The solid is related to steel having following physical characteristics :

- conductivity $k = 25\ W/mK$
- density $\rho = 7700kg/m^3$
- specific heat $C_p = 460J/kgK$

Lower wall's emissivity is fixed to 0.5 and the one of the upper wall at 0.8.

12.1.3 Initial conditions, boundary conditions

Initialy (at $t = 0$), the solid is at $0°C$. We impose on the lower wall a temperature $T_1 = 1000°C$ and on the upper wall a temperature $T_4 = 0°C$.

12.2 Analitycal solution

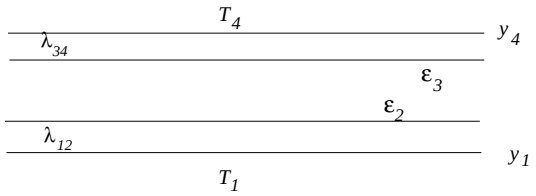

Figure 12.2: 2 parallel plates

In the case of 2 parallel plates, the temperature profile in thickness is given by $T(y) = \varphi\frac{y-y_1}{\lambda_{12}} + T_1$ in the lower part and $T(y) = \varphi\frac{y-y_4}{\lambda_{34}} + T_4$ in the upper part. where φ is a solution of the equation

$$\varphi - \sigma\frac{\varepsilon_2\varepsilon_3}{\varepsilon_2+\varepsilon_3-\varepsilon_2\varepsilon_3}\left[(-\frac{\lambda_{34}}{d_{34}}\varphi + T_4)^4 - (\frac{\lambda_{12}}{d_{12}}\varphi + T_1)^4\right] = 0$$

In the present case we have following datas :

- $\lambda_{12} = \lambda_{34} = 25\ W/mK$
- $\varepsilon_2 = 0.5$, $\varepsilon_3 = 0.8$
- $T_1 = 1000°C$, $T_4 = 0°C$

The previous eqation's solution is then $\varphi = -61070.27839\ W/m^2$

12.3 Calculation description

12.3.1 Meshes

The mesh is realised in 2 dimension.
It has :

- 1782 nodes,
- 784 triangles.

Regarding radiation, the mesh counts 102 facets.
It is closed to both ends by an imposed temperature condition at $0°C$. We assume the domain long enough for this condition has no influence on the channel center where it perfoms comparisons.

12.4 Presentation of results

A calulation was perfomed with a time step equal to 0.3 seconds, which provides a good precision of the transient calculation (altghough only stationary solution could be compared to analytical values, lack of formula discribing transient[1]).

Convergence i sreache about 75 physical seconds representing 250 time steps.

[1] Any proposal of an analytical unstationnary solution for this configuration would be welcome.

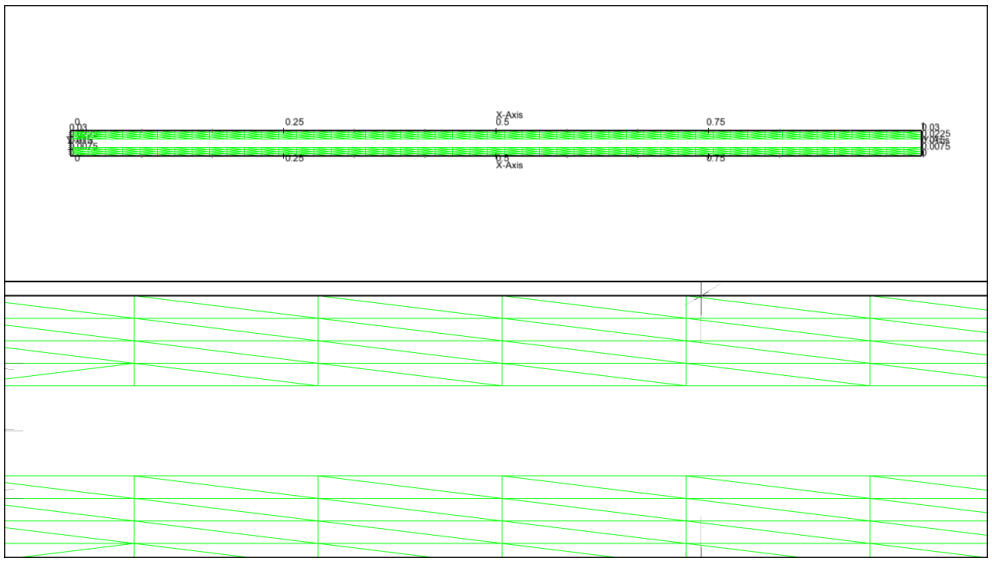

Figure 12.3: Mesh for conduction

12.4.1 Comparison calculation results / analytical value

Comparisons between calculated values and analytical values are made in the middle of the channel in y=0.51.
We can note a very good adequacy between theoretical profiles and values given by SYRTHES.

We can compare temperature values in $y = 0.01$ et $y = 0.02$ (which correspond to inner faces).

Ordinate	analytical T	T SYRTHES
0.01	9.755718886e+02	9.755615295e+02
0.02	2.44281136e+01	2.441899313e+01

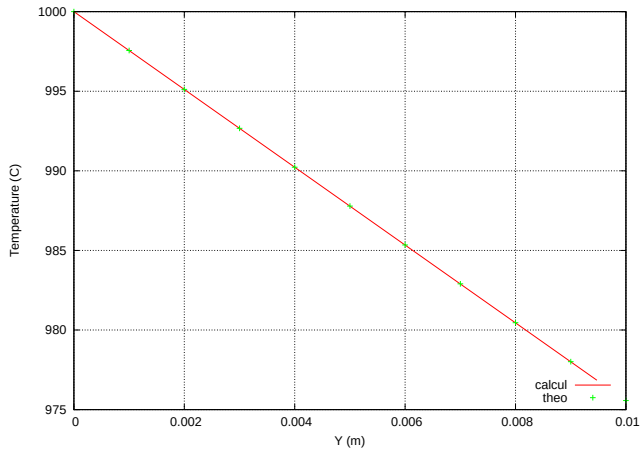

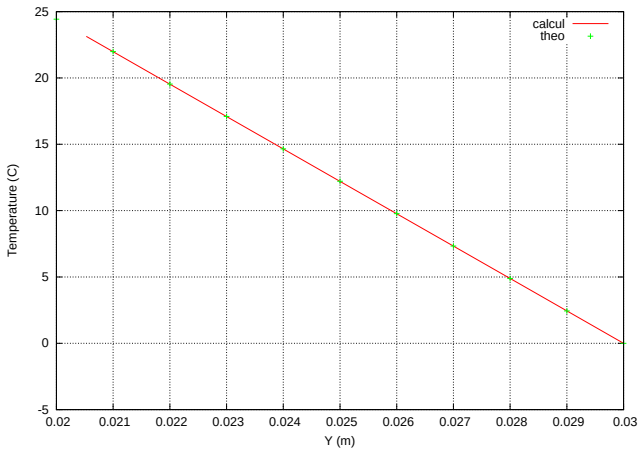

Figure 12.4: Lower wall Upper wall

12.4.2 Thermal field inside plates

The thermal field at convergence is presented on the figure 12.5.

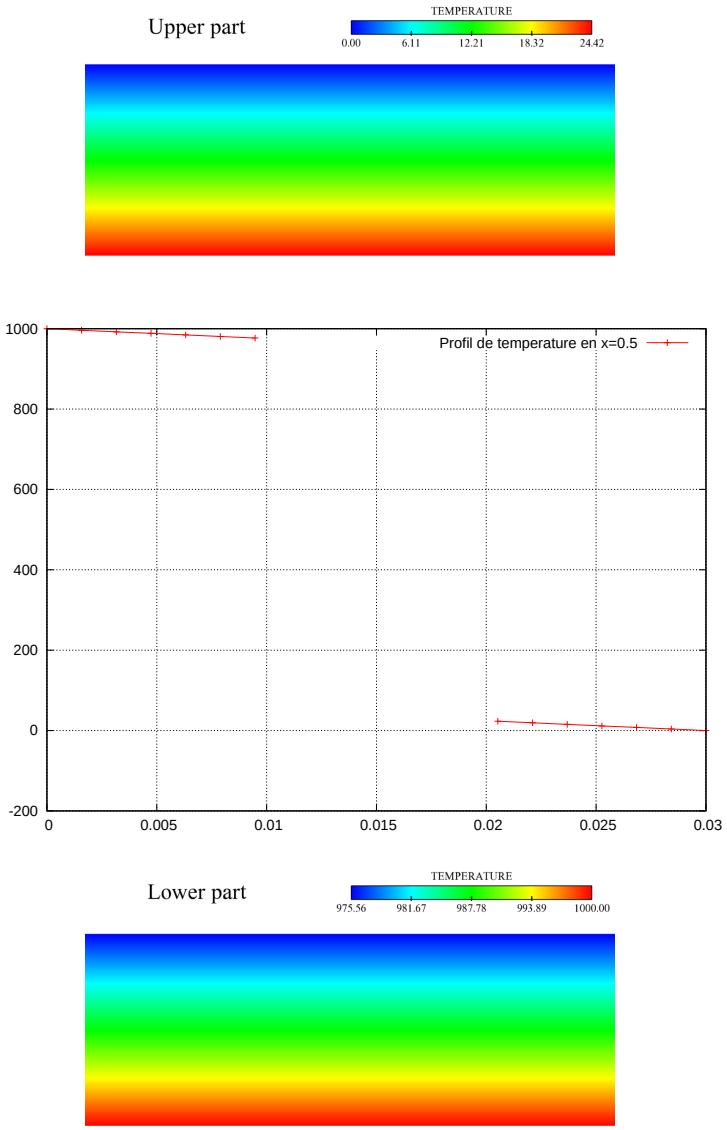

Figure 12.5: Thermal field at convergence

12.4.3 Study of calculation's convergence

The figure 12.4.3 show temperature evolution in 4 points all located in $x = 0.51$ (center of the channel) and respectively at 0.0025 (A), 0.0075 (B), 0.0225 (C), 0.0275(D).

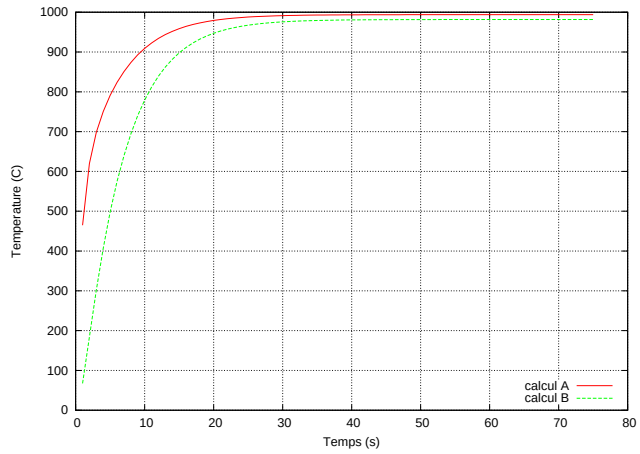

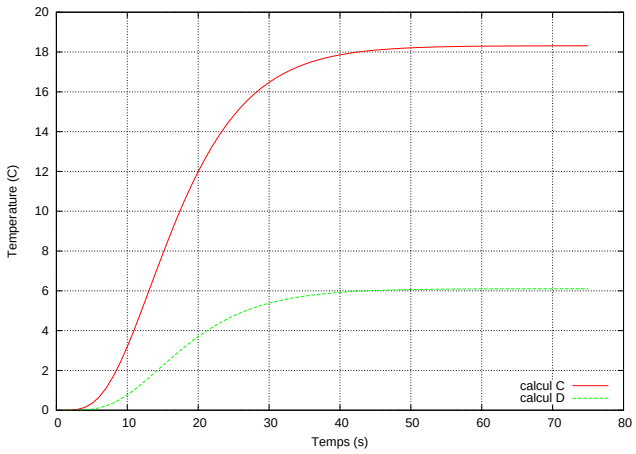

Figure 12.6: Lower wall Upper wall

12.5 Synthesis

Results obtained with SYRTHES on this case are statisfactory.
We could test several aspects :

- meshes reading fo conduction and radiation,
- calculation of view factor in 2D cartesian (faces entirely visible),
- radiative boundary condition and imposed temperature,
- resolution of radiative system,
- resolution of conductive system,
- interpolation between conduction meshes and radiation,
- coupling in conduction and radiation (realised, it reminds, by linearization of radiative exchanges, and treated explicitly).

Chapter 13

CYLINDRES_2D_RAY

Characteristics : Steady state, 2D, cartesian symmetry, coupling conduction/radiation.

Objectives : Validation of radiative calculation in 2D cartesian with shading calculation and consideration of symmetry. Validation of coupling conduction/radiation.

13.1 Test case description

13.1.1 Geometry

Consider two cylindres concentrically nested. Cylinders are considered infinite in length and can be modeled in 2D.

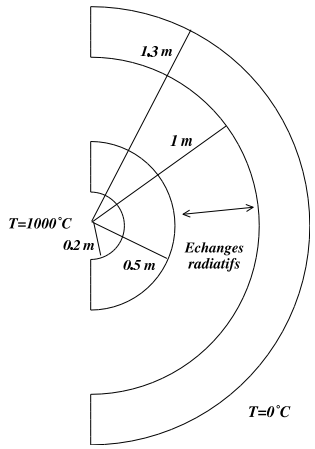

Figure 13.1: Solid domain

13.1.2 Physical conditions

The solid is related to steel having following physical characteristics :

- conductivity $k = 25\ W/mK$
- density $\rho = 7700kg/m^3$
- specific heat $C_p = 460J/kgK$

13.1.3 Initial conditions, boundary conditions

Initialy (at $t = 0$), the solid is at $0°C$. We impose on the inner surface of the inner sphere a temperature $T_1 = 1000°C$ and on outer surface of the outer sphere a temperature $T_4 = 0°C$.

13.2 Analitycal solution

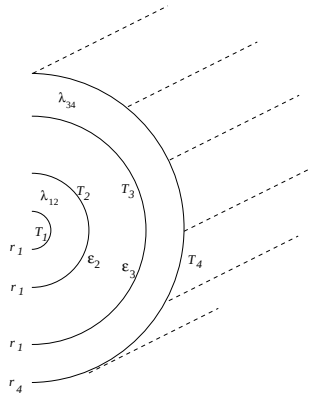

Figure 13.2: 2 infinite concentric cylinder

In the case of 2 concentric cylinder, the flux φ which passes through the surfaces is a solution of the equation

$$\varphi\left(\frac{1}{\varepsilon_2}+\frac{r_2}{r_3}(\frac{1}{\varepsilon_3}-1)\right)-s_2\sigma\left[\left(T_1+\frac{\varphi r_1\log\frac{r_1}{r_2}}{s_1\lambda_{12}}\right)^4-\left(T_4-\frac{\varphi r_4\log\frac{r_3}{r_4}}{s_4\lambda_{34}}\right)^4\right]=0$$

In present case we have following data :

- conductivities $\lambda_{12} = \lambda_{34} = 25\ W/mK$
- emissivities $\varepsilon_2 = 0.5$, $\varepsilon_3 = 0.8$
- edge temperatures $T_1 = 1000°C$, $T_4 = 0°C$
- radii $r_1 = 0.2$, $r_2 = 0.5$, $r_3 = 1.$, $r_4 = 1.3$
- surfaces $s_1 = 2\pi r_1$, $s_2 = 2\pi r_2$, $s_3 = 2\pi r_3$, $s_4 = 2\pi r_4$,

Solution of previous equation is then $\varphi = 59706.82602\ W/m^2$ Then we obtain inner walls temperatures

$$T_2 = T_1 + \varphi\frac{\log\frac{r_1}{r_2}}{2\pi\lambda_{12}} = 651.712890°C$$

$$T_3 = T_4 - \varphi\frac{\log\frac{r_3}{r_4}}{2\pi\lambda_{34}} = 99.7260894°C$$

Temperature profile in a radius of the inner cylinder is given by

$$T(r) = T_1 + \frac{T_1 - T_2}{\log\frac{r_1}{r_2}}\log\frac{r}{r_1}$$

and temperature profile in a radius of the outer cylinder by

$$T(r) = T_4 + \frac{T_3 - T_4}{\log \frac{r_3}{r_4}} \log \frac{r}{r_4}$$

We note of course, that at steady state, solution don't depend on density and heat capacity. These terms change only the thermal inertia of the part and occur only during transient.

13.3 Calculation description

13.3.1 Meshes

In so far as cylinders are supposed of infinite length, we suppose the phenomena in two dimensions and the mesh is then built in 2D.
The mesh has :

- 1 482 nodes with 369 vertex nodes,
- 672 triangles.

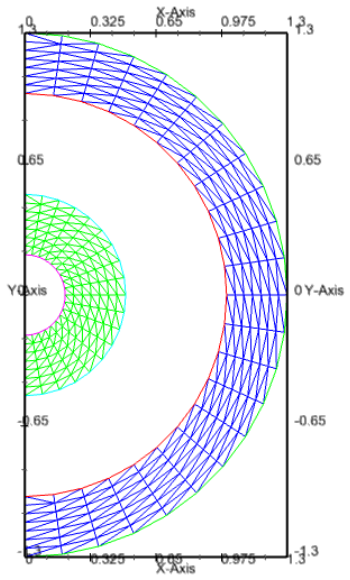

Figure 13.3: Conduction mesh

Note that we use here the sylletry properties which exist in the problem. For conduction, this lead only to impose a null flux. On the other hand, for radiation, it requires that the method can take into account rigorously interaction between the facets of both sides of the plane of symmetry.

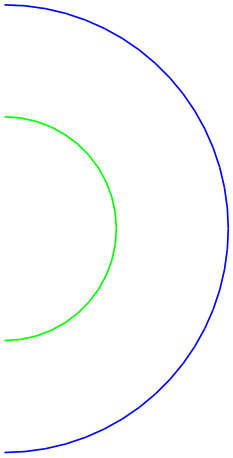

Figure 13.4: Mesh for radiation

Regarding radiation, the mesh is formed by two circular arcs of radius respectively 0.5 m and 1 m. It counts 56 facets.

13.4 Presentation of results

We have performed calculation with a time step equal to 200 seconds.
Convergence has been reached after about 100 000 physical seconds (about 28 hours), with 500 time steps.

13.4.1 Temperature field inside cylinders

We present here the temperature field at convergence.

Figure 13.5: Temperature field at convergence

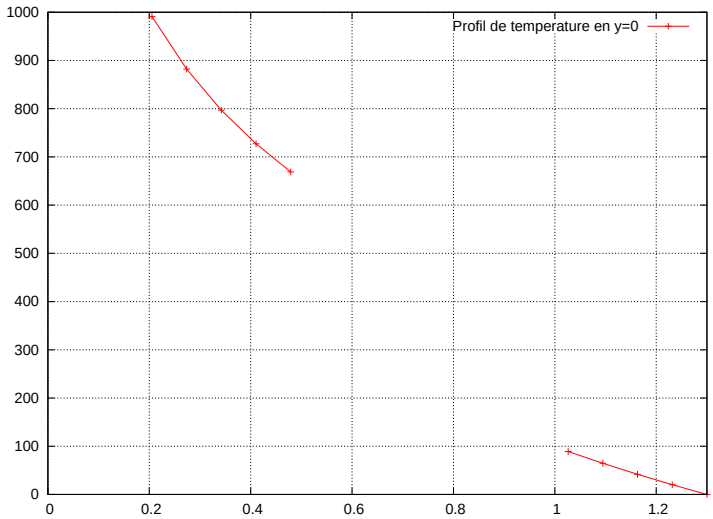

Figure 13.6: Temperature profile at convergence

The figure 13.7 presents temperature domain at convergence but with a temperature which allows to visualize warming of outer cylinder. We also present the temperature profile at y=0.

Note that despite the use of a plane of symmetry, the field obtained complies with the axisymmetric nature of the problem.

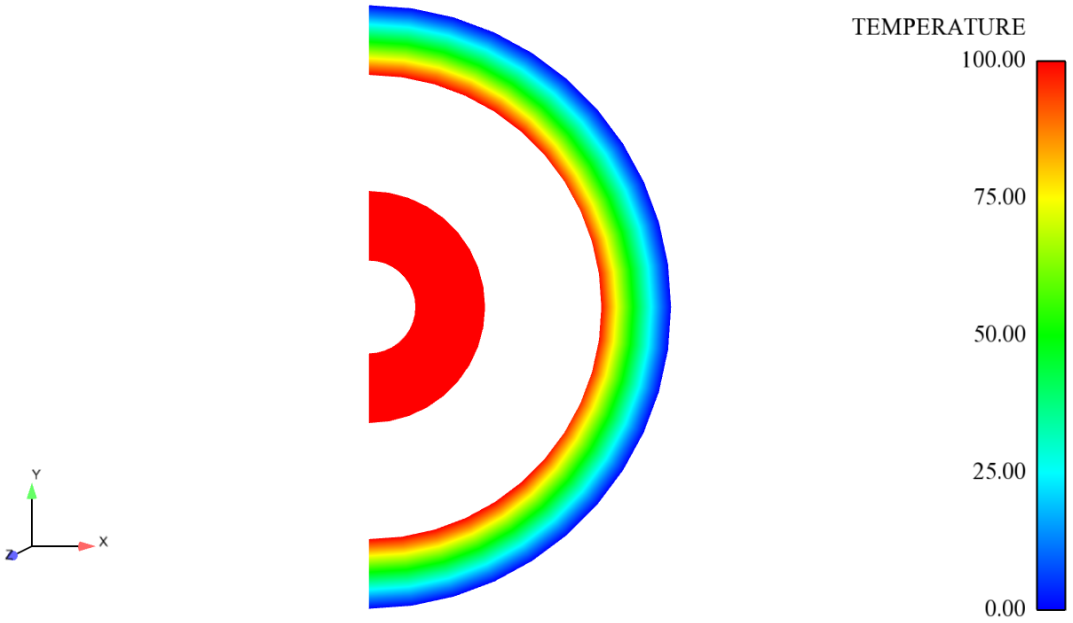

Figure 13.7: Temperature field at convergence

13.4.2 Comparison calculation results / analytical values

Comparisons between calculated values of temperature and analytical values are made along a radius of cylinders.
It may be noted on figure a very good match between the theoretical profiles and values given by SYRTHES.

We can compare temperature values in $r = 0.5$ and $r = 1$

Ordinate	analytical T	T SYRTHES
0.5	6.51712890e+02	6.522676381e+02
1.	9.97260894e+01	9.885848739e+01

Camparisons between analytical profiles and calculated ones

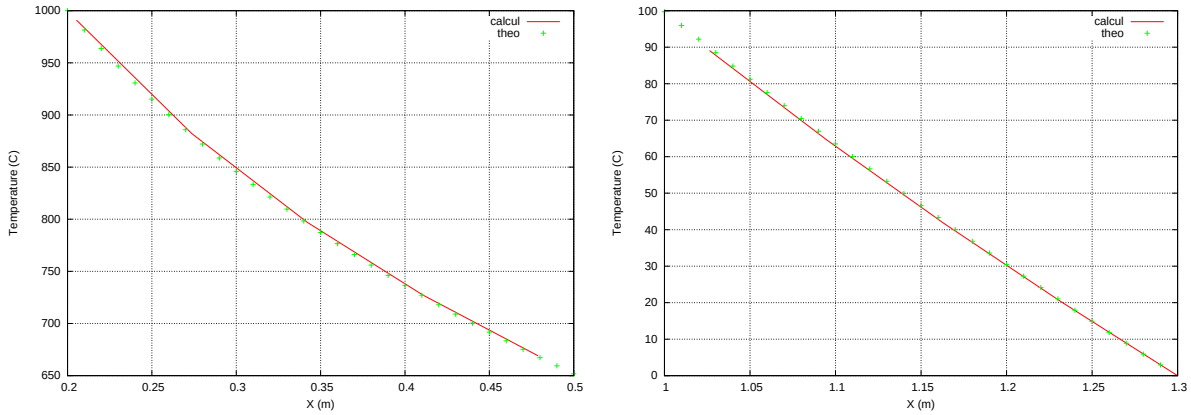

Figure 13.8: Inner cylinder outer cylinder

13.4.3 Study of calculation's convergence

The following figure shows temperature's evolution in 6 points along y=0 : x=0.3 (A), x=0.4 (B), x=0.5 (C), x=1. (D),x=1.1 (E), x=1.2 (F).

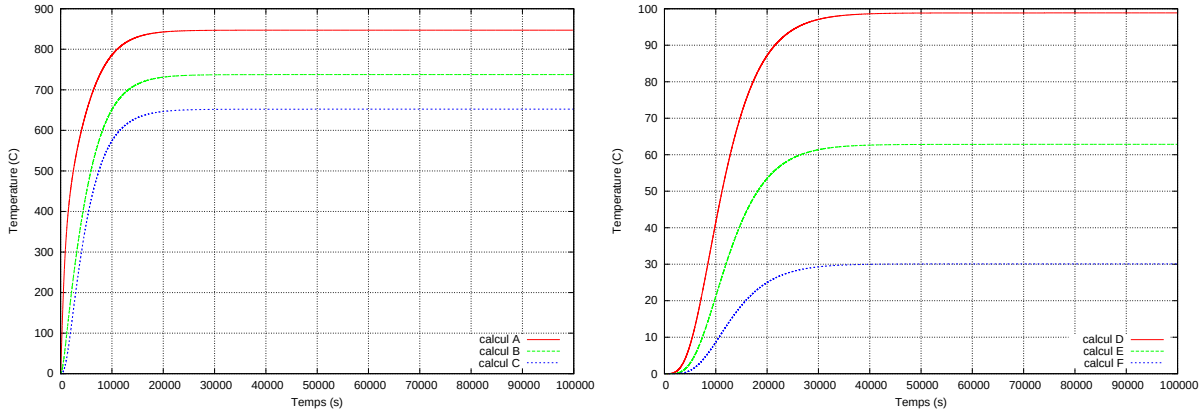

Figure 13.9: Inner cylinder Outer cylinder

The calculation was conducted on a physical time quite long because very small changes in temperature could still be observed after more 70000 physical seconds.

Remarks :

- *Like in the previous case, it would be very useful to have unstationnary analytical solutions for this type of configuration. If they exist, they are probably very complex.*
- *Note that the temperature field obtained complies with the polar nature of the problem, even if a symmetry condition has been used.*

13.5 Synthesis

Results obtained with SYRTHES on this case are statisfactory.
This configuration has allowed to check particularly several aspects :

- calculation of view factor in 2D cartesian,
- calculation of shadowing,
- taking into account of a symmetry. It confirms the harsh treatment of symmetries in radiation,
- calculation of elementary matrices in 2D cartesian,
- coupling in conduction and radiation with a circular interface.

Note that if this configuration appears as if possessing a 1D solution in cylindrical system, it is 2D when it is used in cartesian coordinates as this is the case in SYRTHES.

Chapter 14

SPHERE_RAY

Characteristics : 3D (here represented by a 2D axisymmetric discretization), steady state, coupling conduction/radiation.

Objectives : Validation of radiative calculation in axisymmetric and validation of coupling conduction/radiation.

14.1 Test case description

14.1.1 Geometry

We consider 3 nested hollow spheres :

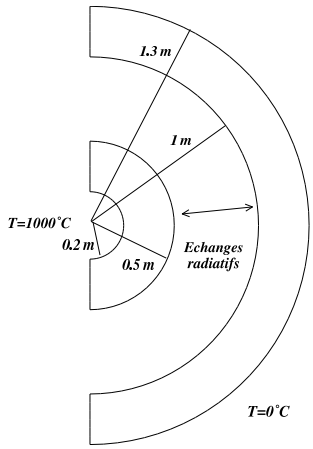

Figure 14.1: Solid domain

14.1.2 Physical conditions

The solid is related to steel having following physical characteristics :

- conductivity $k = 25\ W/mK$
- density $\rho = 7700kg/m^3$
- specific heat $C_p = 460J/kgK$

14.1.3 Initial conditions, boundary conditions

Initialy (at $t = 0$), the solid is at $0°C$. We impose on the inner surface of the inner sphere a temperature $T_1 = 1000°C$ and on the outer surface of the outer sphere a temperature $T_4 = 0°C$.

14.2 Analitycal solution

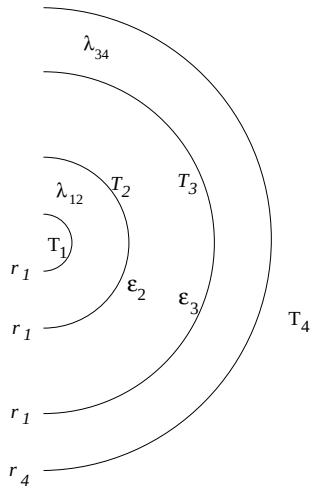

Figure 14.2: 2 concentric spheres

In the case of 2 concentric spheres, the flux φ that passes through the surfaces is solution of the equation

$$\varphi(\frac{1}{\varepsilon_2} + \frac{s_2}{s_3}(\frac{1}{\varepsilon_3} - 1)) - s_2\sigma\left[\left(T_1 + \frac{\varphi r_2^2}{s_2\lambda_{12}}(\frac{1}{r_1} - \frac{1}{r_2})\right)^4 - \left(T_4 - \frac{\varphi r_3^2}{s_3\lambda_{34}}(\frac{1}{r_3} - \frac{1}{r_4})\right)^4\right] = 0$$

In the present case we have following data :

- conductivities $\lambda_{12} = \lambda_{34} = 25\ W/mK$
- emissivities $\varepsilon_2 = 0.5$, $\varepsilon_3 = 0.8$
- edge temperatures $T_1 = 1000°C$, $T_4 = 0°C$
- radii $r_1 = 0.2$, $r_2 = 0.5$, $r_3 = 1.$, $r_4 = 1.3$
- surfaces $s_2 = 4\pi r_2^2$, $s_3 = 4\pi r_3^2$

Solution of previous equation is then $\varphi = 44316.66273 W/m^2$. Then we obtain inner walls temperatures

$$T_2 = T_1 - \frac{\varphi r_2^2(\frac{1}{r_1} - \frac{1}{r_2})}{(s_2\lambda_{12})} = 576.8070439°C$$

$$T_3 = T_4 + \frac{\varphi r_3^2(\frac{1}{r_3} - \frac{1}{r_4})}{(s_3\lambda_{34})} = 32.5533043°C$$

Temperature profile in a radius of the inner sphere is given by

$$T(r) = \frac{T_1 - T_2}{r(\frac{1}{T_1} - \frac{1}{T_2})} + T_1 - \frac{T_1 - T_2}{1 - \frac{r_1}{r_2}}$$

and temperature profile in a radius of the outer sphere by

$$T(r) = \frac{T_3 - T_4}{r(\frac{1}{T_3} - \frac{1}{T_4})} + T_3 - \frac{T_3 - T_4}{1 - \frac{r_3}{r_4}}$$

Like in the previous case (CYLINDRES_2D_RAY), density and heat capacitry disappear at steady state.

14.3 Calculation description

14.3.1 Meshes

The mesh is realised in 2D, it uses axisymmetry property of the problem, this leads to mesh only a slice of spheres.
The mesh counts :

- 1 482 nodes
- 672 triangles

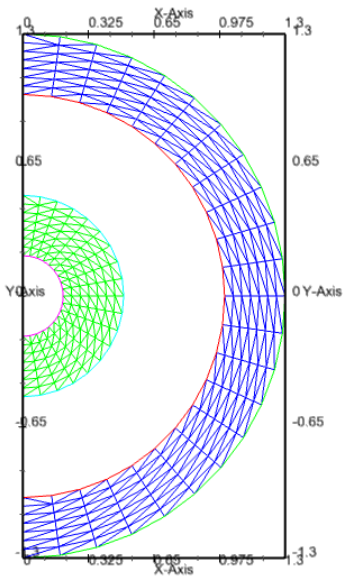

Figure 14.3: Conduction mesh

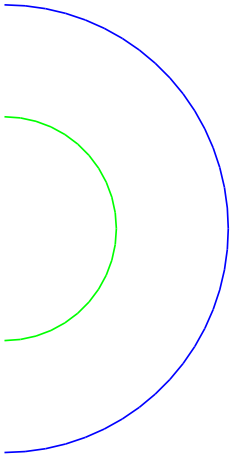

Figure 14.4: Mesh for radiation

Regarding radiation, the mesh is formed by 2 circular arcs of respective radii 0.5 m and 1 m. It counts of 56 faces.

14.4 Presentation of results

We have performed calculation with a time step equal to 200 seconds.
Convergence has been reached after about 100 000 physical seconds (about 28 hours), with 500 time steps.

14.4.1 Temperature field inside the spheres

We present here the temperature at convergence.

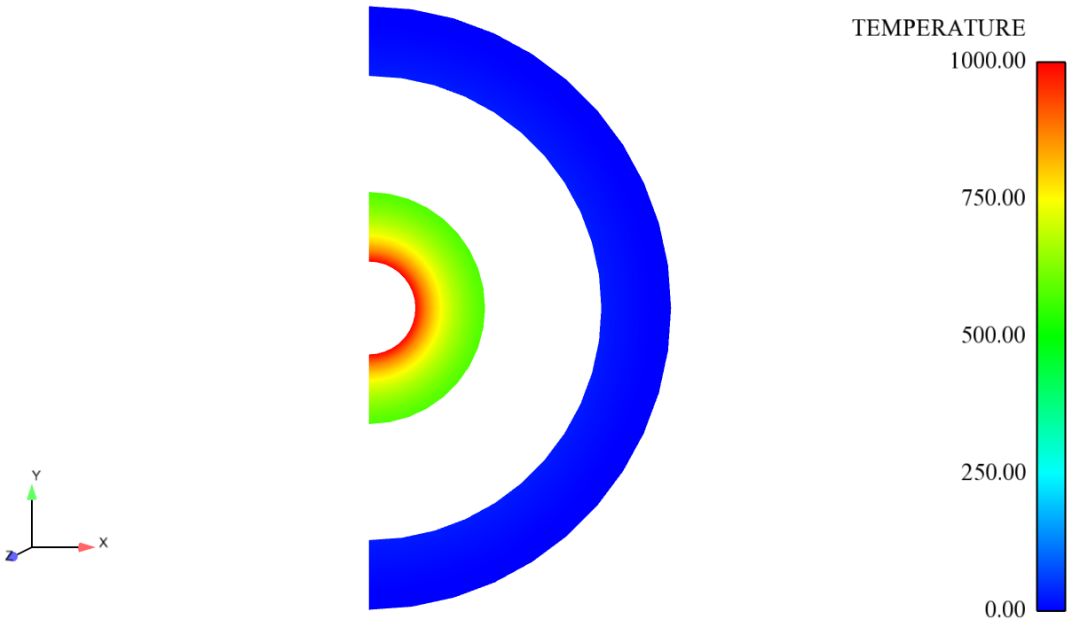

Figure 14.5: Temperature field at convergence

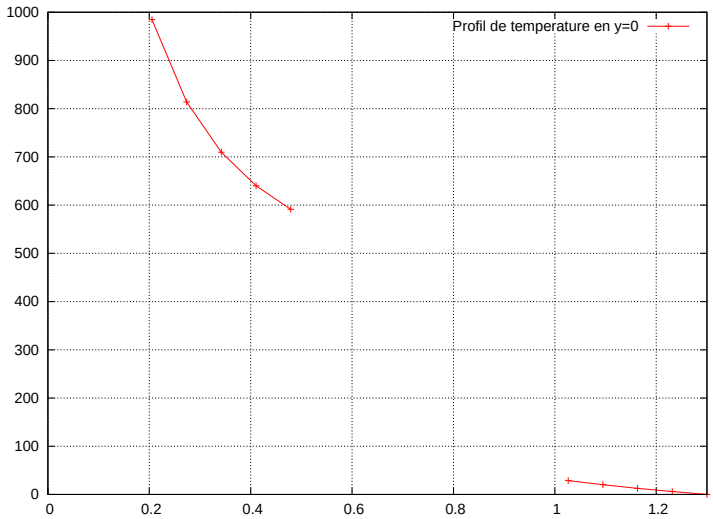

Figure 14.6: Temperature profile at convergence

The figure 14.7 presents temperature domain field at convergence but with a scale which allows to visualize warming of the outer sphere. We also present the temperature profile at y=0.

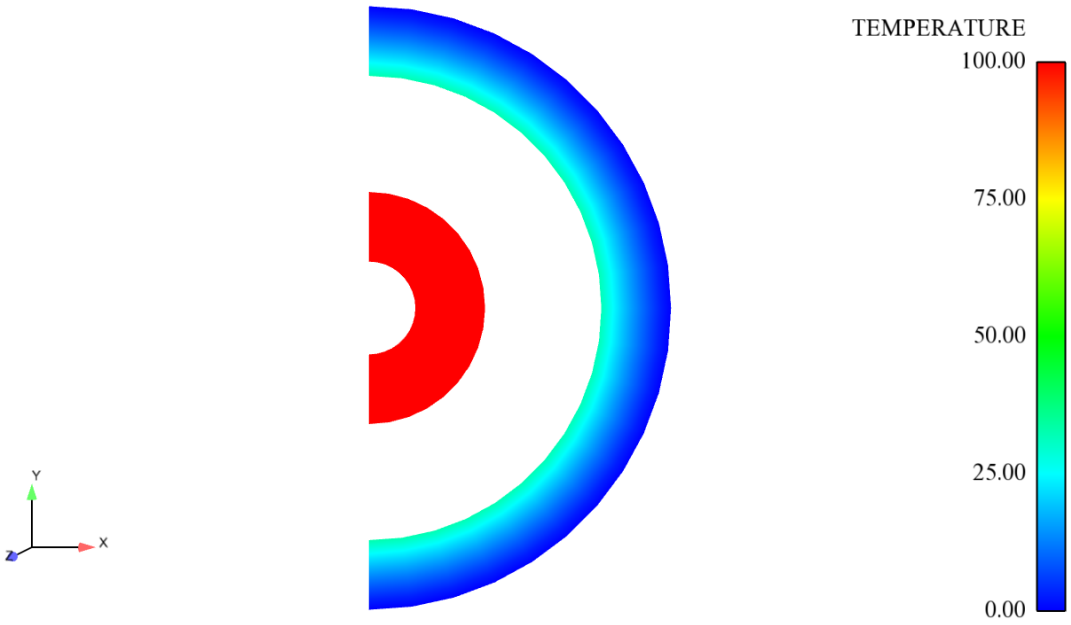

Figure 14.7: Temperature field at convergence

14.4.2 Comparison calculation results / analytical values

Comparisons between calculated values of temperature and analytical values are plotted along a radius of the spheres.

We can compare temperature values in $r = 0.5$ and $r = 1$

Ordinate	analytical T	T SYRTHES
0.5	5.768070439e+02	5.782931957e+02
1.	3.25533043e+01	3.226574813e+01

Remarks :

- *There is an error here slightly more important. It is possible that it is due to the spatial discretization error of the sphere which is approached by faces.*

Camparisons between analytical and calculated profiles

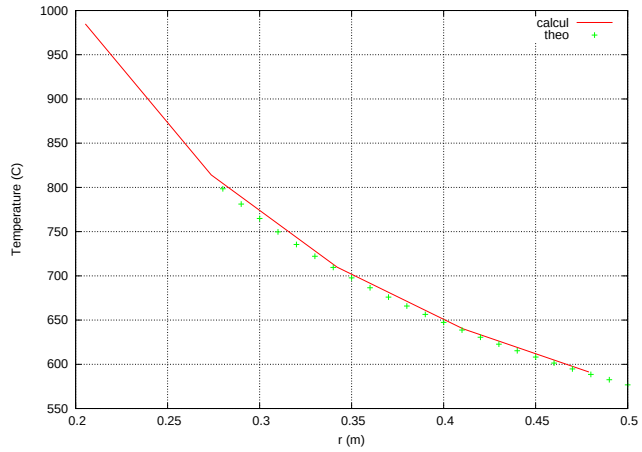

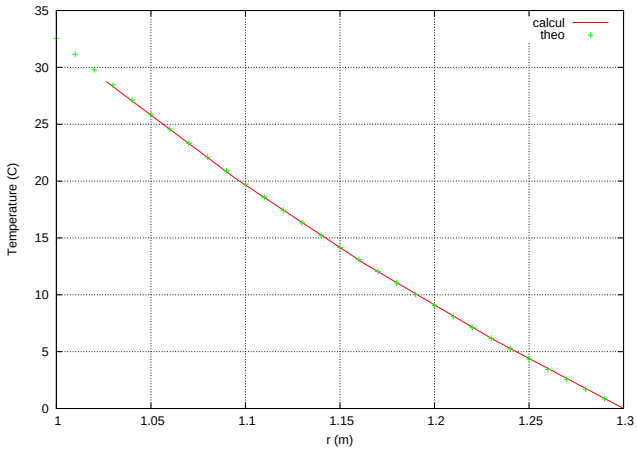

Figure 14.8: Inner sphere Outer sphere

14.4.3 Study of calculation's convergence

The following figure shows temperature's evolution in 6 points along y=0 : x=0.3 (A), x=0.4 (B), x=0.5 (C), x=1. (D),x=1.1 (E), x=1.2 (F).

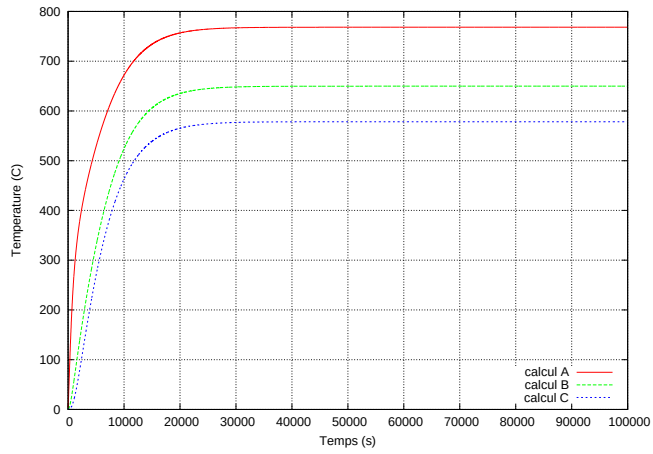

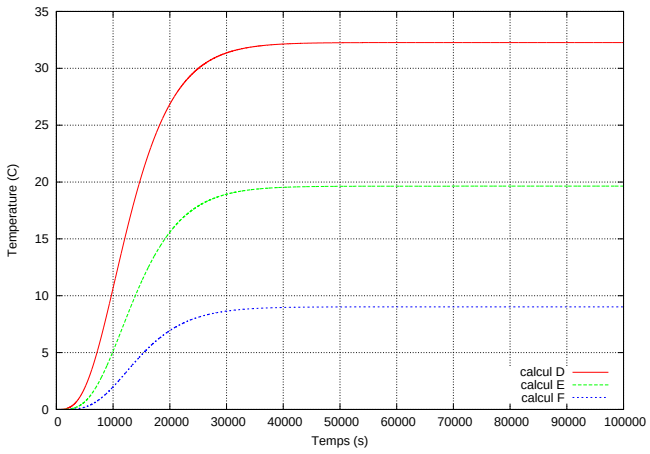

Figure 14.9: Inner sphere Outer sphere

14.5 Synthesis

Results obtained with SYRTHES on this case are statisfactory.
his configuration has allowed to check particularly several aspects :

- calculation of view factors in 2D axisymmetric,
- calculation of shadowing in 2D axisymmetric,
- calculation of elementary matrices in 2D axisymmetric,
- coupling in conduction and radiation in 2D axisymmetric.

Chapter 15

CYLINDRES_3D_RAY

Characteristics : Â£D, steady state, cartesian periodicity, conduction/radiation coupling.

Objectives : Validation of radiative calculation in 3D cartesian with shadowing calculation and taking into account of periodicity of rotation. Validation of conduction/radiation coupling.

15.1 Test case description

15.1.1 Geometry

Consider two concentric cylinder. Cylinders are assumed of infinite length and are modeled in 3D. For calculation, we chose a sufficient length in order to minimize influence of radiative boundary condition which is necessary to give at the ends of the domain.

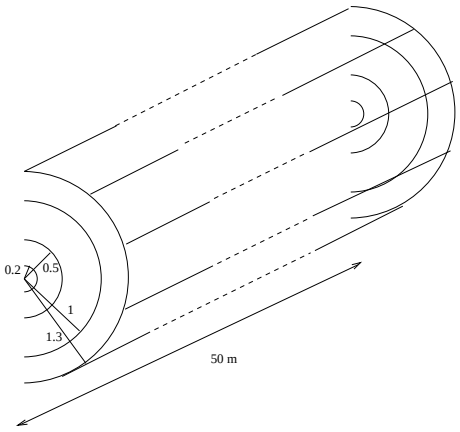

Figure 15.1: Solide domain

15.1.2 Physical conditions

The solid is related to steel having following physical characteristics :

- conductivity $k = 25\ W/mK$
- density $\rho = 7700 kg/m^3$
- specific heat $C_p = 460 J/kgK$

15.1.3 Initial conditions, boundary conditions

Inititialy (at $t = 0$), the solid is at $0°C$. We impose on the inner surface of the inner cylinder a temperature $T_1 = 1000°C$ and on the outer surface of the outer cylindera temperature $T_4 = 0°C$.

15.2 Analitycal solution

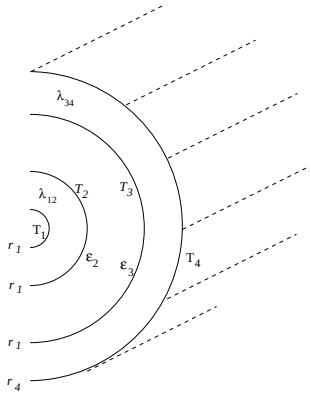

Figure 15.2: 2 infinite concentric cylinder

In the case of 2 concentric cylinder, the flux φ which passes through the surfaces is a solution of the equation

$$\varphi\left(\frac{1}{\varepsilon_2}+\frac{r_2}{r_3}(\frac{1}{\varepsilon_3}-1)\right)-s_2\sigma\left[\left(T_1+\frac{\varphi r_1\log\frac{r_1}{r_2}}{s_1\lambda_{12}}\right)^4-\left(T_4-\frac{\varphi r_4\log\frac{r_3}{r_4}}{s_4\lambda_{34}}\right)^4\right]=0$$

In present case we have following data :

- conductivities $\lambda_{12} = \lambda_{34} = 25\ W/mK$
- emissivities $\varepsilon_2 = 0.5$, $\varepsilon_3 = 0.8$
- edge temperatures $T_1 = 1000°C$, $T_4 = 0°C$
- radii $r_1 = 0.2$, $r_2 = 0.5$, $r_3 = 1.$, $r_4 = 1.3$
- surfaces $s_1 = 2\pi r_1$, $s_2 = 2\pi r_2$, $s_3 = 2\pi r_3$, $s_4 = 2\pi r_4$

Solution of previous equation is then $\varphi = 59706.82602\ W/m^2$
Then we obtain inner walls temperatures

$$T_2 = T_1 + \varphi\frac{\log\frac{r_1}{r_2}}{2\pi\lambda_{12}} = 651.712890°C$$

$$T_3 = T_4 - \varphi\frac{\log\frac{r_3}{r_4}}{2\pi\lambda_{34}} = 99.7260894°C$$

Temperature profile in a radius of the inner cylinder is given by

$$T(r) = T_1 + \frac{T_1 - T_2}{\log\frac{r_1}{r_2}}\log\frac{r}{r_1}$$

and temperature profile in a radius of the outer cylinder by

$$T(r) = T_4 + \frac{T_3 - T_4}{\log\frac{r_3}{r_4}}\log\frac{r}{r_4}$$

15.3 Calculation description

15.3.1 Meshes

The mesh is realised in 3D. Wer have meshed 1/8 of cylinders.
Conditions of periodicity are used during calculation.
The mesh has :

- 51 408 nodes,
- 33630 tetrahedra.

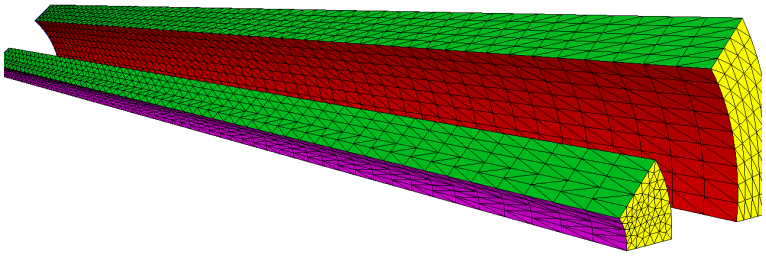

Figure 15.3: Mesh for conduction

Regarding radiation, the mesh consist of 2012 facets. In order to close the domain, we impose at both ends a null flux condition (in order to minimize influence of extremities).

Remarks :
In this 3D case, space discretization is coarser than in the 2D case seen in previous paragraph. Indeed, the radiation mesh has already 2012 facets for 1/8 domain this will lead to view factor calculation for some 16096 facets even if, ultimately, only 2 025 078 view factors will be stored (instead of calculation and storage of the 129 548 656 view factors if the whole domain had been meshed !)

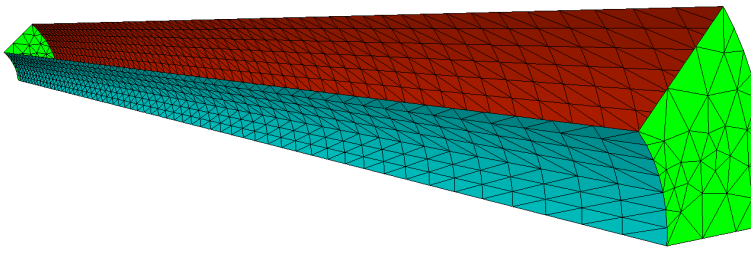

Figure 15.4: Radiation mesh

15.4 Presentation of results

We have performed calculation with a time step equal to 200 seconds.
Convergence has been reached after about 100 000 physical seconds (about 28 hours), with 500 time steps.

15.4.1 Temperature domains inside cylinders

We present here the temperature field at convergence.

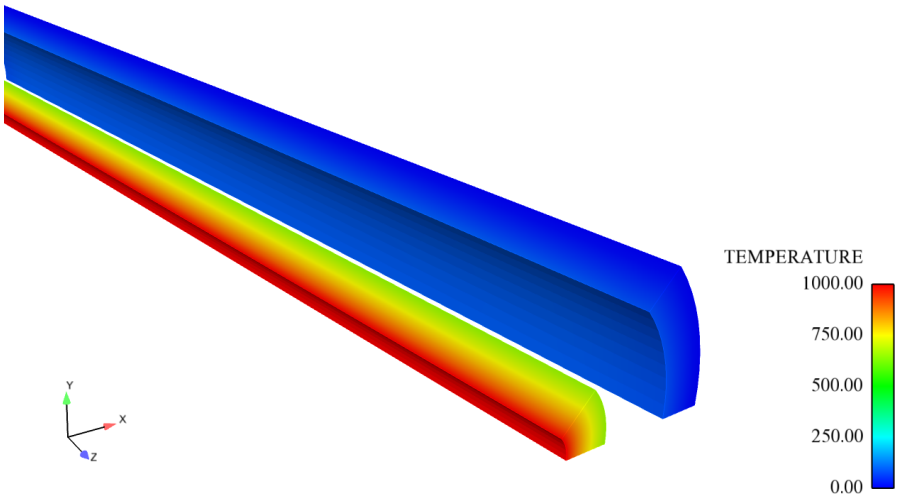

Figure 15.5: Temperature domain at convergence

The figure 15.6 present temperature domain at convergence but with different scales which allow to visualize isotherms inside inner and outer cylinders.

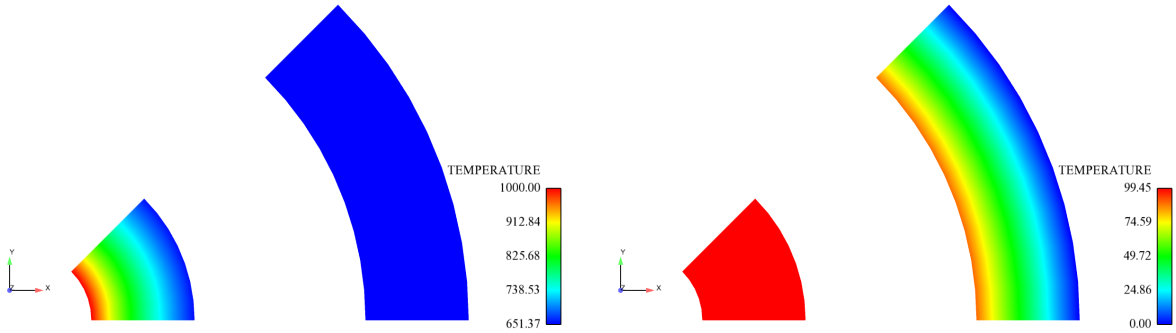

Figure 15.6: Temperature domain at convergence

15.4.2 Comparison calculation results / analytical values

Comparisons between calculated values of temperature and analytical values are made along a radius of cylinders. Following profiles present also comparisons between 2D calculation (see the test case "CYLINDRES_2D_RAY") and this calculation in 3D.

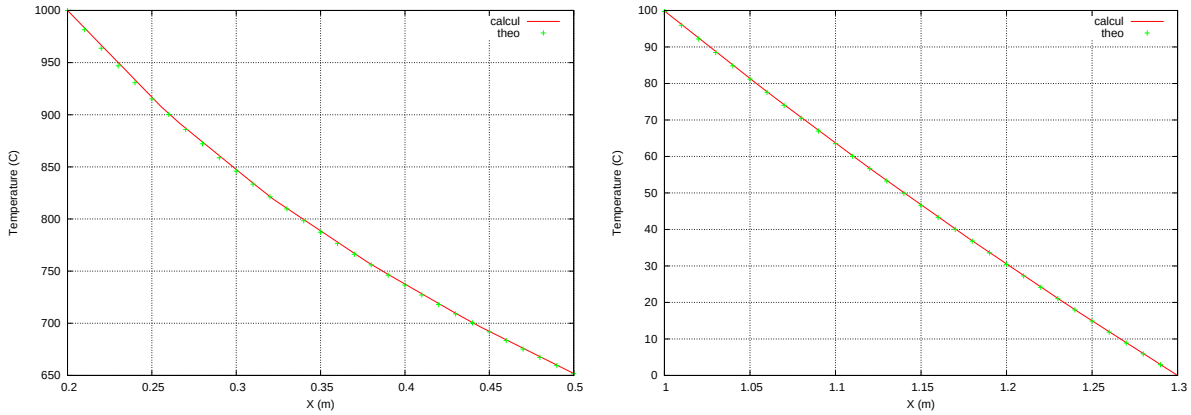

Figure 15.7: Inner cylinder Outer cylinder

15.4.3 Study of calculation's convergence

The following figure shows temperature's evolution in 6 points along y=0 : x=0.26 (A), x=0.32 (B), x=0.5 (C), x=1. (D),x=1.12 (E), x=1.24 (F).

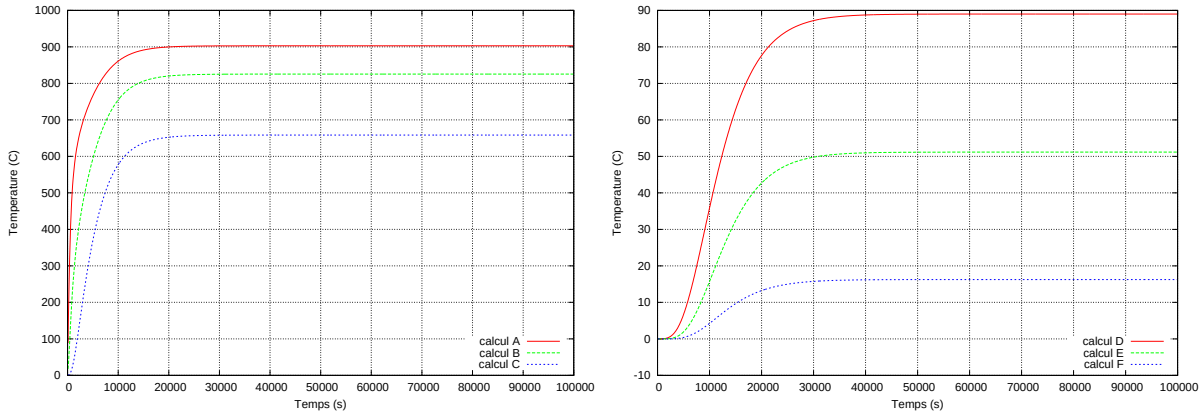

Figure 15.8: Inner cylinder Outer cylinder

15.5 Synthesis

Results obtained with SYRTHES on this case are statisfactory.
It should be noted that this configuration is much more heavier to use because it's necessary a domain of great length in oder to minimize effect of boundary conditions to the ends. We have then numbers of nodes and facets relatively large.

This configuration has allowed to check several aspects particularly :

- conduction mesh reading (volumetric) and radiation (surface) in 3D,
- calculation of view factor in 3D,
- calculation of shadowing in 3D,
- taking into account of periodicity. Note the good result, related to the fact that periodicity is treated rigorously. In this particular case, the benefit of time and of memory space is

significant : we compute and store 8×2012×2013/2=16 200 624 quad integrals instead of 16096×16097/2=129 548 656 if integrality of the domain had been meshed.

- consideration of coupling and null flux boundary conditions (on the ends),
- calculation of elementary conduction matrices in 3D,
- numerical coupling in conduction and radiation.

It should be noted that similar remarks to those made in the test case "ANNEAU" concerning faceting of the structure can be made. Add to this the fact that analytical solution implies an infinitely long domain along cylinders's axis. Here infinite length introduce an "inaccuracy" in the distribution of energy (even if it remains modest because of the length modeled).

Part III

TRANSFERTS COUPLES

Chapter 16

WOODPANEL

Characteristics : Wall with boundary conditions constants TÂ ; pv

Objectives : We wish to estimate the profile of temperature and humidity in a timber insulation board of medium density insulation board. It is located in a theoretical situation, where the boundary conditions are constant for each side wall (outer atmosphere, and internal conditions), and wherein the upper and lower faces are isolated (heat and moisture).

16.1 Test case description

16.1.1 Geometry

The wall is made exclusively of a wood fiber material of medium density, with a height of 1 meter. The outer faces are flat and parallel. The wall thickness of 8 cm.

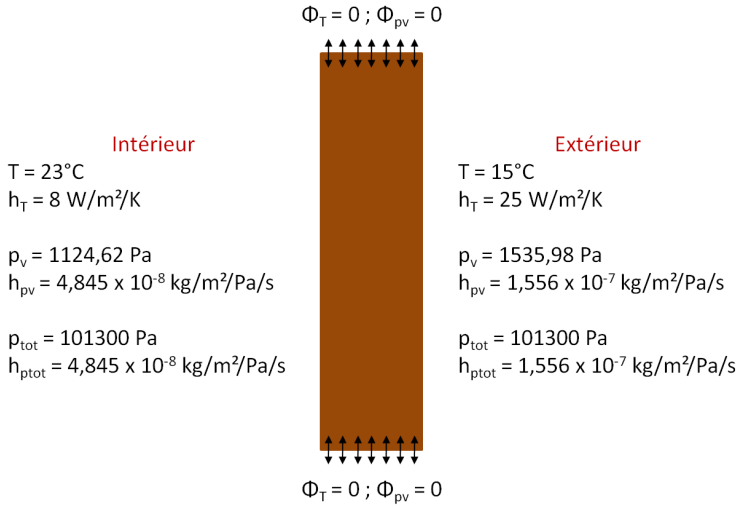

Figure 16.1: Solide domain

16.1.2 Physical conditions

In all material, the initial conditions are :

- $T = 23°C$

- $p_v = 1124,62Pa$

16.1.3 Boundary conditions

The boundary conditions are :

Ambiance	$T(°C)$	h_T $(W/m^2/K)$	p_v (Pa)	h_{pv} $(kg/m^2/s/Pa)$	p_t (Pa)	h_{pt} $(kg/m^2/s/Pa)$
Indoor	23	8	1124.6	$4.845\ 10^{-8}$	101300	$4.845\ 10^{-8}$
Outdoor	15	25.1	1535.98	$1.556\ 10^{-7}$	101300	$1.556\ 10^{-7}$

16.2 Calculation description

16.2.1 Meshes

The mesh is realised in 2d. The mesh counts :
The mesh has :

- 6 320 nodes,
- 12 324 triangles.

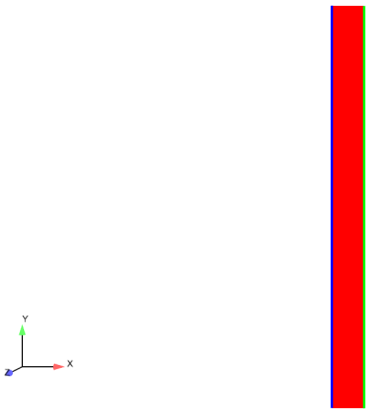

Figure 16.2: Solid mesh

The mesh references are

Description	Type	Reference
A timber insulation board MDF	Volume (material)	1
Ambiance outdoor	Surface (boundary condition)	1
Ambiance indoor	Surface (boundary condition)	2
Flux null, on the upper and lower faces of the panel	Surface (boundary condition)	0

16.3 Presentation of results

We have performed calculation with a time step equal to 60 seconds.Convergence has been reached after about 6105 physical seconds (about 6,95 days), with 10000 time steps.
we consider the following results, reports every hour:

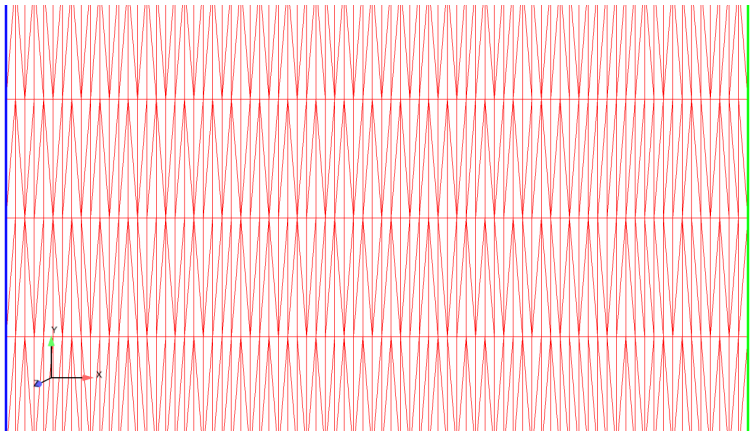

Figure 16.3: Zoom solid mesh

- Changes in temperature and humidity depending on the thickness of the panel (all cm)
- Field temperatures at the end of the simulation
- Field vapor pressures, HR and volumetric water rates at the end of the simulationâ
- Mass balances in the volume

In a statement every hour, use the frequency output: "Every time steps n '= 60, and the contact information of the following sensors:

- Sonde 1 : (0 ; 0.5)
- Sonde 2 : (0.01 ; 0.5)
- Sonde 3 : (0.02 ; 0.5)
- Sonde 4 : (0.03 ; 0.5)
- Sonde 5 : (0.04 ; 0.5)
- Sonde 6 : (0.05 ; 0.5)
- Sonde 7 : (0.06 ; 0.5)
- Sonde 8 : (0.07 ; 0.5)
- Sonde 9 : (0.08 ; 0.5)

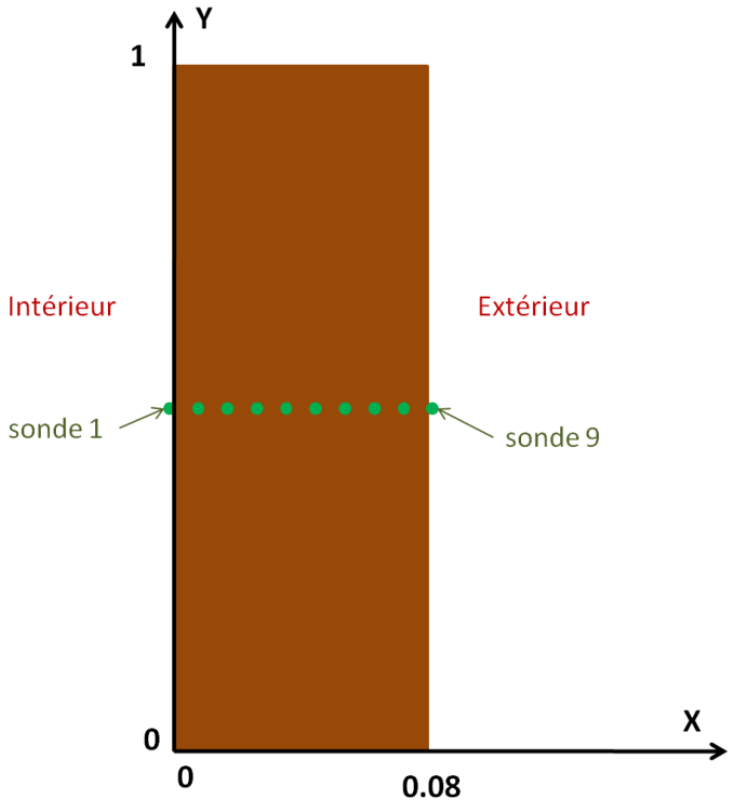

Figure 16.4: Sondes

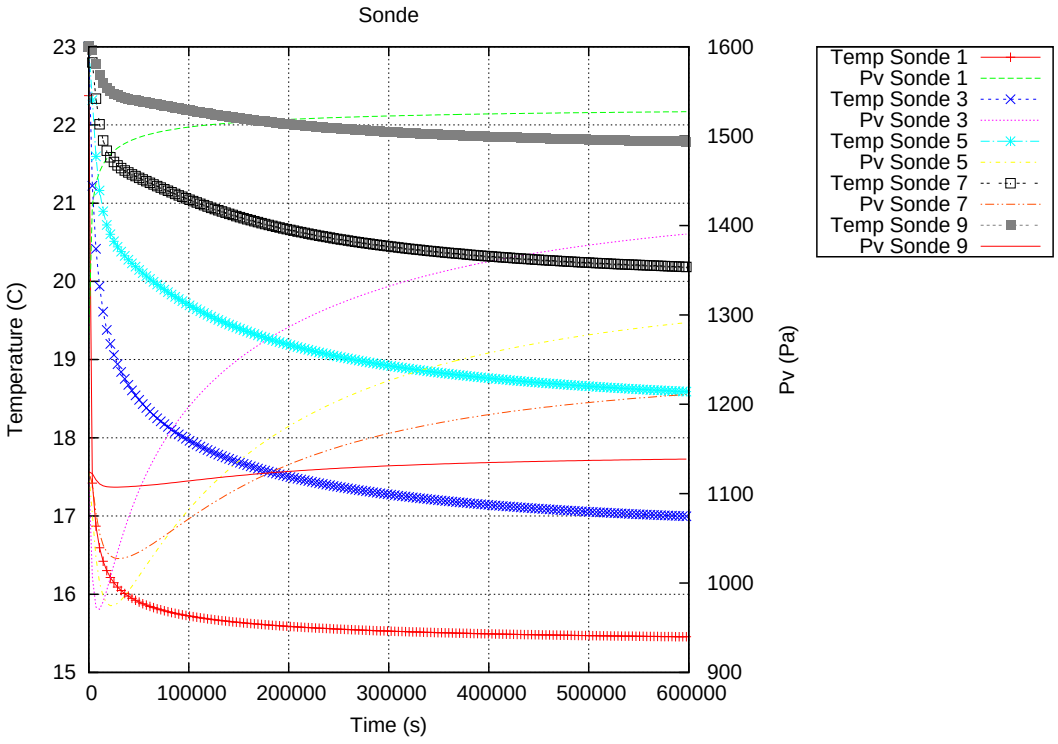

Figure 16.5: Sondes

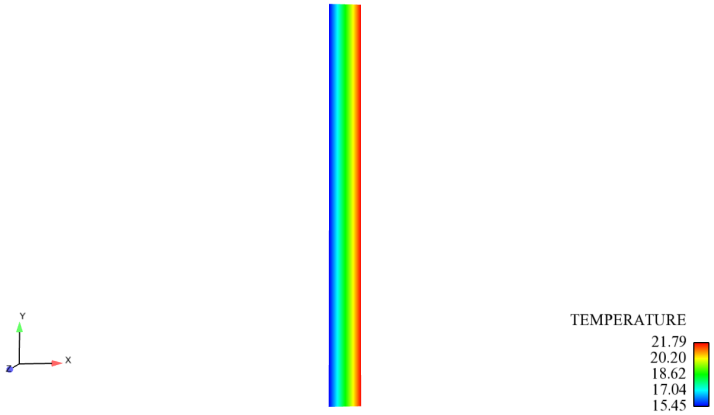

Figure 16.6: temperature domain at convergence

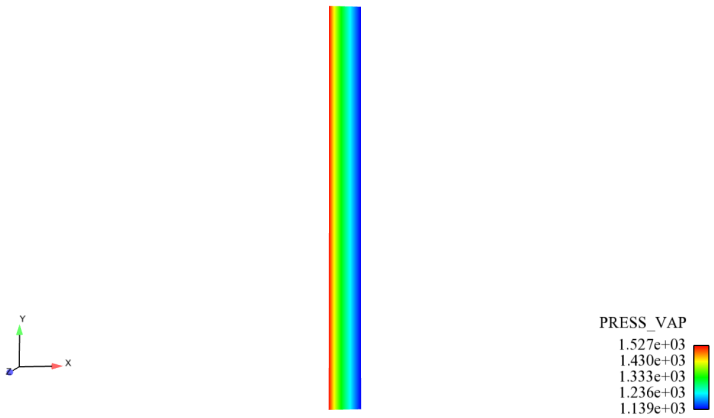

Figure 16.7: pressure vapour domain at convergence

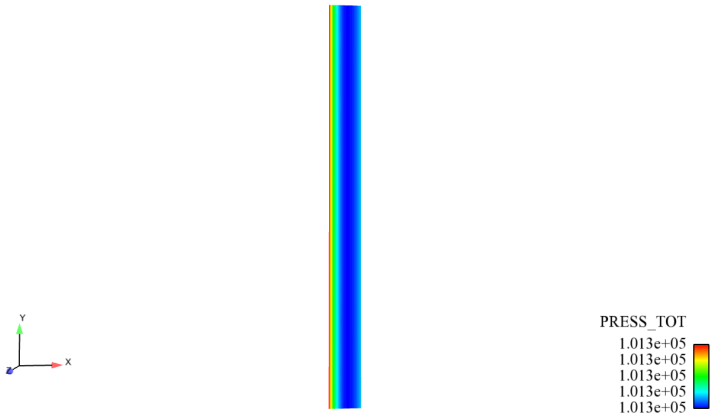

Figure 16.8: pressure total domain at convergence

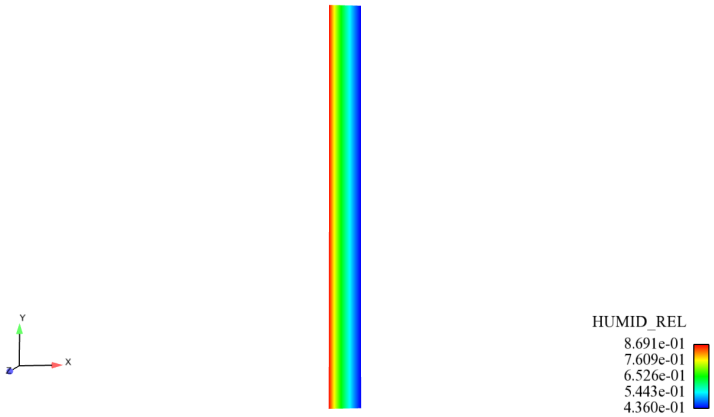

Figure 16.9: relative humidity domain at convergence

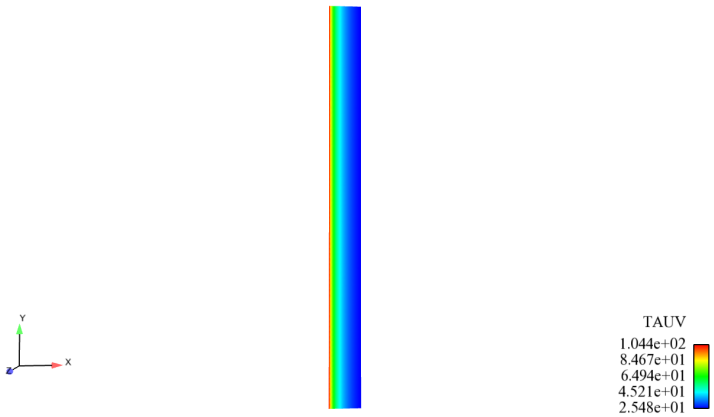

Figure 16.10: volumic moiture level domain at convergence

Bibliography

[1] Péniguel C. Heat transfer simulation for industrial applications : Needs, limitations, expectations. pages 102–114. Int Journal of Heat and Fluid Flow (vol 19), Elsevier, 1998.

[2] Rupp I , Péniguel C. Coupling heat conduction and radiation and convection phenomena in complex 2D and 3D geometries. U.K. Swansea, 1997. Numerical Methods in Thermal Problems.

[3] Rupp I , Péniguel C. Coupling heat conduction, radiation and convection in complex geometries. Int Journal of Numerical Methods for Heat and Fluid Flow - Vol 9, 1999.

[4] Rupp I, Péniguel C. *Manuel utilisateur du code Syrthes 3.1.* Rapport EDF/DER HE-41/97/052/A.

[5] Rupp I, Péniguel C. *SYRTHES - Conduction et rayonnement thermique - Manuel théorique de la version 3.1.* Rapport EDF/DER HE-41/98/048A.

[6] Sparrow E M, CESS R D. *Radiation Heat Transfer.*

[7] Péniguel C , Rupp I. Coupling conduction radiation and convection using PVM. St Venant Symp. Paris, 1997.

[8] Péniguel C, Rupp I. A numerical method for thermally coupled fluid and solid problems. pages 1027–1039, U.K. Swansea, 1993. Numerical Methods in Thermal Problems.

[9] Péniguel C, Rupp I. A finite element approach to simulate general conduction problems. pages 555–562, U.K. Southampton, 1994. 3rd Int Conference Heat Transfer.

[10] Péniguel C, Rupp I. A numerical approach for thermally coupled fluid and solid problems in complex geometries. pages 27–34, U.K. Southampton, 1994. 3rd Int Conference Heat Transfer.

[11] Péniguel C, Rupp I. A numerical approach of coupled heat conduction and enclosure radiation problems. pages 787–796, Italy - Venezia, 1995. 8th FEMIF.

[12] Péniguel C, Rupp I. A numerical approach of thermal problems coupling fluid solid and radiation in complex geometries. pages 797–806, Italy - Venezia, 1995. 8th FEMIF.

[13] Péniguel C, Rupp I. Coupling heat conduction and radiation in complex 2D and 3D geometries. U.K. Swansea, 1997. Numerical Methods in Thermal Problems.

[14] Carslow HS, Jaeger JC. *Conduction of Heat in Solids.* Second edition, Oxford University Press, 1959.

[15] Siegel R, Howell JR. *Thermal Radiation Problem.* Second edition, Hemisphere Publishing Corporation, New York.